Cell Chemical Biology
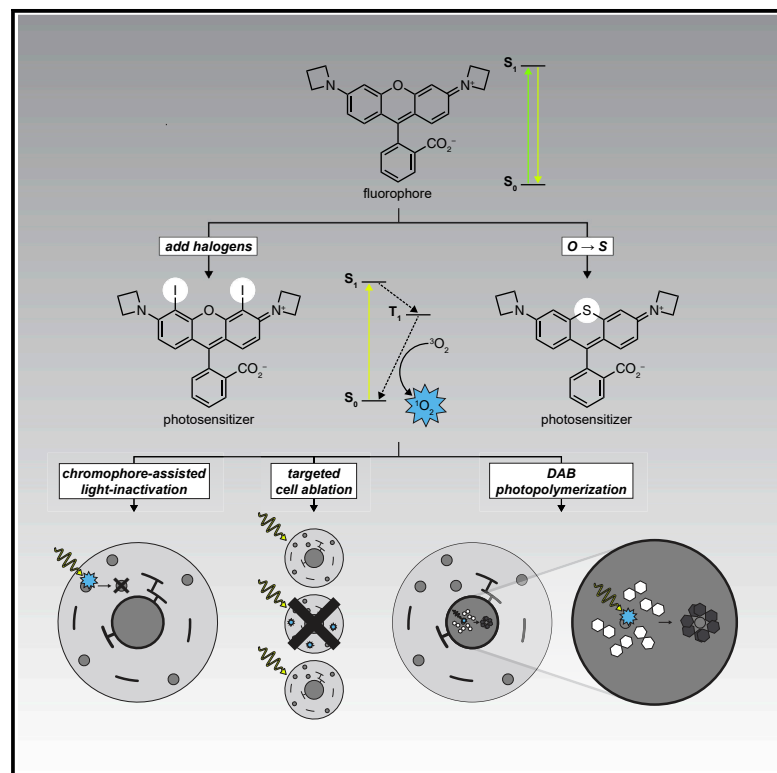
Rational Design of Bioavailable Photosensitizers for Manipulation and Imaging of Biological Systems

Graphical Abstract

Authors

Thomas C. Binns, Anthony X. Ayala, Jonathan B. Grimm, ...,
Mark H. Ellisman, Minoru Koyama, Luke D. Lavis

Correspondence

lavisl@janelia.hhmi.org

In Brief

Binns et al. describe photosensitizers based on rhodamine dyes. Incorporation of halogen or sulfur atoms into the rhodamine structure substantially increases singlet oxygen quantum yield. Combined with the HaloTag-labeling system, these photosensitizers allow light-mediated destruction of proteins, ablation of entire cells, or deposition of electron microscopy contrast agents.

Highlights

- Incorporation of iodine or sulfur into rhodamine dyes increases $^1O_2$ quantum yield

- Rhodamine photosensitizers are compatible with live-cell-labeling strategies

- Generating $^1O_2$ allows photoablation of entire cells in culture or *in vivo*

- Photopolymerization of 3,3′-diaminobenzidine gives contrast in electron microscopy

CelPress

Resource

Rational Design of Bioavailable Photosensitizers for Manipulation and Imaging of Biological Systems

Thomas C. Binns,[1,2,3] Anthony X. Ayala,[1] Jonathan B. Grimm,[1] Ariana N. Tkachuk,[1] Guillaume A. Castillon,[4] Sebastien Phan,[4] Lixia Zhang,[1] Timothy A. Brown,[1] Zhe Liu,[1] Stephen R. Adams,[5] Mark H. Ellisman,[4] Minoru Koyama,[1] and Luke D. Lavis[1,6,*]

[1]Janelia Research Campus, Howard Hughes Medical Institute, Ashburn, VA 20147, USA
[2]Graduate School, University of Arkansas for Medical Sciences, Little Rock, AR 72205, USA
[3]College of Medicine, University of Arkansas for Medical Sciences, Little Rock, AR 72205, USA
[4]Department of Neurosciences, University of California San Diego, La Jolla, CA 92093, USA
[5]Department of Pharmacology, University of California San Diego, La Jolla, CA 92093, USA
[6]Lead Contact
*Correspondence: lavisl@janelia.hhmi.org
https://doi.org/10.1016/j.chembiol.2020.07.001

SUMMARY

Light-mediated chemical reactions are powerful methods for manipulating and interrogating biological systems. Photosensitizers, compounds that generate reactive oxygen species upon excitation with light, can be utilized for numerous biological experiments, but the repertoire of bioavailable photosensitizers is limited. Here, we describe the synthesis, characterization, and utility of two photosensitizers based upon the widely used rhodamine scaffold and demonstrate their efficacy for chromophore-assisted light inactivation, cell ablation in culture and *in vivo*, and photopolymerization of diaminobenzidine for electron microscopy. These chemical tools will facilitate a broad range of applications spanning from targeted destruction of proteins to high-resolution imaging.

INTRODUCTION

The ability to measure and manipulate biological systems using light-driven processes has revolutionized biology. The excited state that occurs after a molecule absorbs light can be harnessed in different ways. Fluorescent dyes absorb and then emit light of different wavelengths, allowing sensitive visualization of biological processes inside cells. Photoactivatable ("caged") compounds use the excited state energy to break chemical bonds and release bioactive molecules with high spatiotemporal precision. Optogenetic reagents use light to drive conformational changes in proteins to affect cellular function. Finally, photosensitizing molecules absorb light energy and then transfer it to adjacent molecules, facilitating specialized chemistries inside cells and tissue.

A key application of photosensitizers is the generation of reactive oxygen species (ROS) through the interaction of the triplet excited state of the photosensitizer with molecular oxygen ($^3O_2$) (Baptista et al., 2017; Xiong et al., 2019). The resulting singlet oxygen ($^1O_2$) and other ROS can be leveraged to manipulate or interrogate biological systems in a variety of ways: chromophore-assisted light inactivation (CALI) of proteins, targeted ablation of cells, or photooxidation and subsequent polymerization of diaminobenzidine (DAB) to provide contrast in light and electron microscopy (EM). This broad utility has led to the development of different classes of photosensitizers useful in living systems. Small-molecule photosensitizers fall into three main classes: por-

phyrins and phthalocyanines, transition-metal complexes, and fluorescent dyes appended with heavy atoms (Xiong et al., 2019). Extant compounds possess excellent photophysical properties but often exhibit limited bioavailability and can be difficult to target to specific cells or subcellular regions. Recent work on genetically encoded photosensitizers based on flavoproteins has produced useful reagents, such as miniSOG, that can be expressed in specific cells or subcellular regions (Bulina et al., 2006; Riani et al., 2018; Ruiz-Gonzalez et al., 2013; Shu et al., 2011), but these protein-based photosensitizers have relatively short excitation wavelengths (Torra et al., 2019). KillerRed and SuperNova are protein-based photosensitizers with longer excitation wavelengths and well-documented utility (de Rosny and Carpentier, 2012; Takemoto et al., 2013), but their potency is lower than small-molecule photosensitizers (Onukwufor et al., 2020).

We set out to develop a hybrid small molecule:protein photosensitizer system that combines the flexibility and performance of small-molecule dyes with the subcellular specificity of genetically encoded reagents. To complement the recent development of impressive noncovalent hybrid photosensitizer systems (He et al., 2016; Marek and Davis, 2002; Tour et al., 2003) based on labeling strategies that require a constant supply of small-molecule ligand (Ayele et al., 2019), we aimed to use the covalent HaloTag-labeling system developed by Promega (Los et al., 2008). This "self-labeling" enzyme-derived tag system has been used in many contexts ranging from single cells (Chong et al., 2018) to animals (Abdelfattah et al., 2019) and
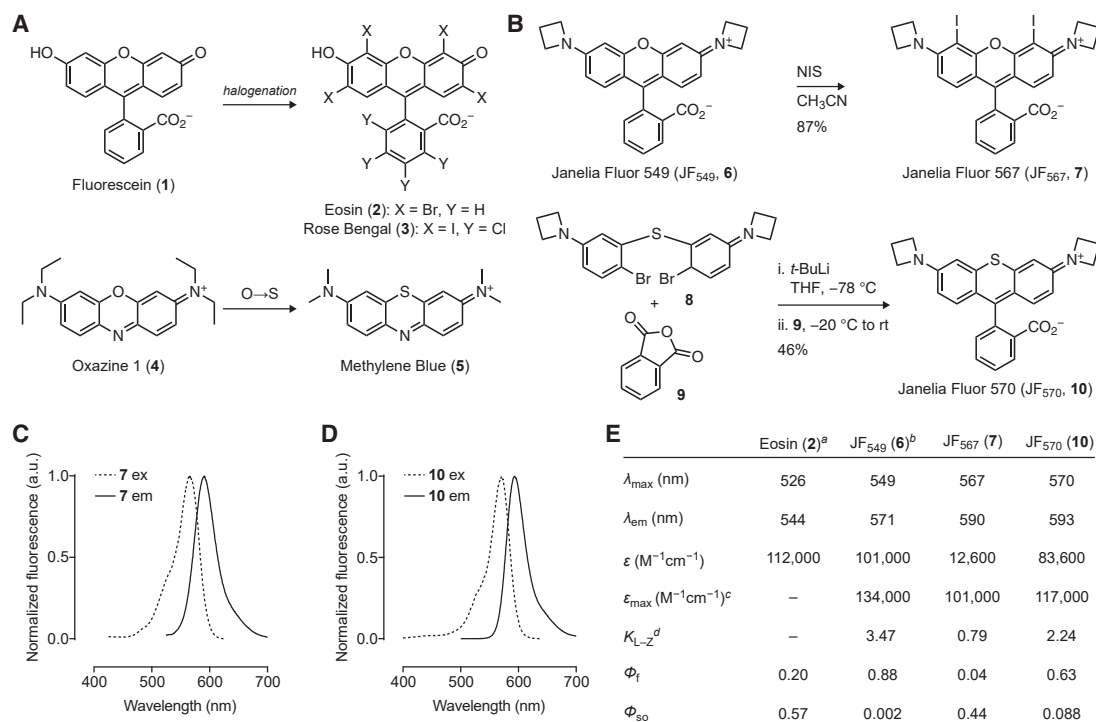
Figure 1. Photosensitizer Structures, Synthesis, and Photophysical Characterization

(A) Relationship of classic photosensitizer chemical structures to parent fluorophores. Eosin (**2**) and Rose Bengal (**3**) are halogenated derivatives of fluorescein (**1**) and methylene blue (**5**) is a sulfur-containing analog of oxazine 1 (**4**).

(B) Iodination of JF$_{549}$ (**6**) to yield JF$_{567}$ (**7**) and organolithium-mediated reaction of **8** and **9** to yield JF$_{570}$ (**10**).

(C and D) Normalized fluorescence excitation (ex) and emission (em) spectra of (C) **7** and (D) **10**.

(E) Table of photophysical properties for eosin (**2**), JF$_{549}$ (**6**), JF$_{567}$ (**7**), and JF$_{570}$ (**10**).

Notes: [a]data for **2** taken from (Fleming et al., 1977; Gandin et al., 1983; Seybold et al., 1969); [b]data for **6** taken from (Grimm et al., 2015, 2017b); [c]ϵ_{max} measured in trifluoroethanol + 0.1% (v/v) trifluoroacetic acid; and [d]K_{L-Z} measured in 1:1 (v/v) dioxane:water.

	Eosin (**2**)[a]	JF$_{549}$ (**6**)[b]	JF$_{567}$ (**7**)	JF$_{570}$ (**10**)
λ_{max} (nm)	526	549	567	570
λ_{em} (nm)	544	571	590	593
ϵ (M^{-1}cm^{-1})	112,000	101,000	12,600	83,600
ϵ_{max} (M^{-1}cm^{-1})[c]	–	134,000	101,000	117,000
K_{L-Z}[d]	–	3.47	0.79	2.24
Φ_f	0.20	0.88	0.04	0.63
Φ_{so}	0.57	0.002	0.44	0.088

provides rapid, specific labeling of protein fusions with synthetic fluorophores. Previous examples of HaloTag-compatible photosensitizers are typically fluorescein derivatives, such as eosin (Figure 1A) and related compounds. Such ligands are excited by relatively short wavelengths (Lee et al., 2008; Li et al., 2018; Takemoto et al., 2011), which are phototoxic on their own (Douthwright and Sluder, 2017; Magidson and Khodjakov, 2013), and require ester-masking groups to render the molecules cell permeable (Takemoto et al., 2011). We now report HaloTag-compatible photosensitizer ligands based on our cell- and tissue-permeable azetidine-containing "Janelia Fluor" rhodamine scaffold (Grimm et al., 2015, 2017b). These dyes are red shifted compared with eosin and do not need ester-masking groups for membrane permeability. We demonstrate the utility of these probes for CALI, targeted cell ablation in culture and *in vivo*, and photoinduced DAB deposition for EM. This work expands the repertoire of the HaloTag-labeling system to ablation of cells in intact animals and generating contrast for EM.

RESULTS

Rational Design and Synthesis of Janelia Fluor Photosensitizers

Many classic small-molecule photosensitizers exploit the "heavy atom effect" (Gold, 1987), where the incorporation of an atom with a relatively high atomic number enhances the rate of intersystem crossing from the singlet excited state to the triplet excited state. This triplet state then interacts with molecular oxygen ($^3O_2$), generating singlet oxygen ($^1O_2$) with concomitant relaxation of the dye to the ground state; the efficiency of singlet oxygen generation can be quantified as the singlet oxygen quantum yield (Φ_{SO}). This principle is illustrated by the halogenation of fluorescein (**1**, Φ_{SO} = 0.03) to yield classic photosensitizers eosin (i.e., eosin Y; **2**, Φ_{SO} = 0.57) and Rose Bengal (**3**, Φ_{SO} = 0.76, Figure 1A), where the halogen substituents also shift the absorption wavelengths to the red (Fleming et al., 1977; Gandin et al., 1983; Seybold et al., 1969). Likewise, replacement of the oxygen in the phenoxazine dyes, such as laser dye oxazine 1 (**4**), with sulfur yields well-known photosensitizer methylene blue (**5**, Figure 1A) (Becker et al., 1990; Francisco et al., 2017). This substitution also elicits a bathochromic shift in wavelength with the increase in Φ_{SO}.

We sought to apply this heavy atom effect to rhodamine dyes, which are widely used fluorescent labels but have received limited attention as photosensitizer scaffolds (Pal et al., 1996). A key advantage of rhodamine dyes over fluorescein-based compounds, such as eosin (**2**) and Rose Bengal (**3**), is based on charge. Fluorescein derivatives are anionic at physiological pH and, as highlighted above, require ester-masking groups to allow efficient entry into cells. These ester bonds are notoriously

unstable in aqueous solution, particularly for halogenated derivatives such as **2** and **3** (Lavis et al., 2006, 2011); their use *in vivo* typically requires injection of DMSO solutions directly into tissue (Sawinski et al., 2009). In contrast, simple rhodamine dyes are net neutral and exist in equilibrium between a lipophilic lactone and polar zwitterion. This "dynamic amphipathicity" allows rhodamines to rapidly traverse biological membranes without the need for auxiliary groups, allowing facile loading into living cells and even animals (Abdelfattah et al., 2019; Grimm et al., 2017b). We recently developed an improved class of rhodamines, the Janelia Fluor dyes, which incorporate four-membered azetidine rings in place of the common dimethylamino groups found in many classic rhodamines. This simple substitution results in substantial improvements in photophysical properties (Grimm et al., 2015) and facilitates rational fine-tuning of the spectral and chemical features of these molecules (Grimm et al., 2017b). For example, the prototypical Janelia Fluor 549 (JF_{549}, **6**, Figure 1B) exhibits a 2-fold improvement in both brightness and photostability in cellular-imaging experiments compared with the parent tetramethylrhodamine compound (Grimm et al., 2015). Since increased excited state lifetime and photostability are important for photosensitizer performance, we sought to extend this azetidine-incorporation strategy to photosensitizer dyes. We envisioned either halogenation (à la **3**) or sulfur substitution (à la **5**) applied to rhodamine compounds, such as **6**. For the halogenation strategy, we found that straightforward treatment of JF_{549} (**6**) with *N*-iodosuccinimide afforded compound **7** with incorporation of two iodine atoms at the 4- and 5-positions of the xanthene moiety (Figure 1B). To accomplish the sulfur substitution, we adapted our recent synthetic approach to rhodamine dyes (Grimm et al., 2017a) through lithium-bromide exchange of brominated diarylthioether **8** followed by addition to phthalic anhydride (**9**) to yield compound **10** (Figure 1B).

We then examined the spectral and chemical properties of these two dyes compared with eosin (**2**) and JF_{549} (**6**; Figures 1C–1E). As in other halogenated xanthene dyes (e.g., **2** and **3**), the iodo substituents in rhodamine **7** elicited a bathochromic shift with an absorption maximum (λ_{max}) of 567 nm and an emission maximum (λ_{em}) of 590 nm in aqueous buffer; we named this dye "Janelia Fluor 567" (JF_{567}) based on the λ_{max}. Likewise, the replacement of the bridging oxygen with a sulfur in **10** caused a red shift in its spectra with $\lambda_{max}/\lambda_{em}$ = 570 nm/593 nm; we gave this dye the moniker "Janelia Fluor 570" (JF_{570}). We then investigated the absorptivity of these dyes in aqueous solution. Although the sulfur-containing JF_{570} (**10**) showed high absorptivity with an extinction coefficient (ϵ) of 83,600 M^{-1} cm^{-1}, the halogenated derivative JF_{567} (**7**) gave a substantially lower ϵ = 12,600 M^{-1} cm^{-1}. As mentioned above, rhodamines exist in equilibrium between a colorless, nonfluorescent lactone form, and a colored, fluorescent zwitterionic form. We suspected that the electron-withdrawing iodo substituents in compound **7** shifted this equilibrium toward the colorless lactone form. We therefore measured the equilibrium constant ($K_{L–Z}$) and maximum extinction coefficient (ϵ_{max}) using trifluoroethanol containing 0.1% (v/v) trifluoroacetic acid, a solvent system that promotes formation of the open form (Grimm et al., 2017b; Zheng et al., 2019) (Figure 1E). Under these conditions we found that both dyes exhibit high absorptivity (ϵ_{max} > 100,000 M^{-1} cm^{-1}), demonstrating that the difference in observed ϵ in aqueous solution is due to a shift in

the lactone-zwitterion equilibrium and not significant differences in the inherent absorptivity of the two chromophores.

We then measured the fluorescence quantum yield (Φ_f) and singlet oxygen quantum yield (Φ_{SO}) of both potential photosensitizer dyes using Rose Bengal (**3**; Φ_{SO} = 0.76) (Ezquerra Riega et al., 2017) as a standard. JF_{567} (**7**) showed a relatively low Φ_f = 0.04 and a high Φ_{SO} = 0.44. In contrast, JF_{570} (**10**) showed a higher Φ_f = 0.63 balanced by a more modest Φ_{SO} = 0.088. These Φ_{SO} values were substantially higher than the parent fluorophore JF_{549} (**6**), which gave a low Φ_{SO} = 0.002. For comparison, eosin (**2**) has a reported Φ_{SO} = 0.57 (Gandin et al., 1983) and the Φ_{SO} for methylene blue (**5**) has been measured at 0.07 in aqueous solution (Francisco et al., 2017). These data show that both halogenation and sulfur substitution substantially increase Φ_{SO} compared with the parent dye and that these Φ_{SO} values are comparable with those of established photosensitizers, such as eosin and methylene blue.

Synthesis of HaloTag Ligands and CALI

To enable attachment of these dyes to specific proteins in living systems, we prepared derivatives of both **7** and **10** containing the chloroalkane HaloTag ligand moiety at the optimal **6**-position on the pendant phenyl ring (**7HTL** and **10HTL**; Figure 2A) (Los et al., 2008). These were synthesized in analogous fashion to the free dyes. The JF_{567}-HaloTag ligand (**7HTL**; Figure S1A) involved direct iodination of 6-carboxy-JF_{549} (**11**) to give the diiodo 6-carboxy-JF_{567} (**12**), which could be amidated with the HaloTag ligand amine (**13**) to yield **7HTL**. The synthesis of **10HTL** was more involved (Figure S1B), starting with the coupling of 3-bromothiophenol (**14**) and 3-bromoiodobenzene (**15**) to give diarylthioether **16**. Cross-coupling with azetidine gave **17**, which was regioselectively brominated with NBS to give **8**. Metalation of **8** with *t*-BuLi and addition to diorthoester methyl benzoate **18** followed by deprotection gave 6-carboxy-JF_{570} (**19**). Amidation with the HaloTag ligand amine (**13**) yielded **10HTL**.

We evaluated the properties of **7HTL** and **10HTL** (Figure 2A) as conjugates with purified HaloTag protein (HT) *in vitro*. The equilibrium between the open, colored zwitterionic form and the closed, colorless lactone of rhodamine dyes can be leveraged to create chromogenic and fluorogenic ligands—molecules that show large increases in absorption and fluorescence upon binding their cognate biomolecular target. Since JF_{567} (**7**) exhibited a relatively low extinction coefficient in aqueous solution and a relatively low $K_{L–Z}$ (Figure 1E), we predicted that the JF_{567}-HaloTag ligand (**7HTL**) would show increased absorption upon binding the HaloTag protein. Indeed, incubation of this photosensitizer dye with HaloTag protein elicited an 8.6-fold increase in absorption due to binding of the ligand to the HaloTag protein (Figure 2B), similar in magnitude to the prototypical fluorogenic rhodamine dye tetramethyl-Si-rhodamine (Lukinavicius et al., 2013). In contrast, the JF_{570}-HaloTag ligand did not show a substantial increase in absorption (Figure 2C), as expected from the properties of the free dye (Figure 1E). We further investigated the properties of the HaloTag conjugates and compared them with eosin-HaloTag ligand (**2HTL**); this was prepared by treatment of the commercially available diacetate compound (**2HTLAc2**) (Takemoto et al., 2011) with porcine liver esterase (Figures 2D and S2A). JF_{567}-HaloTag ligand (**7HTL**) and JF_{570}-HaloTag ligand
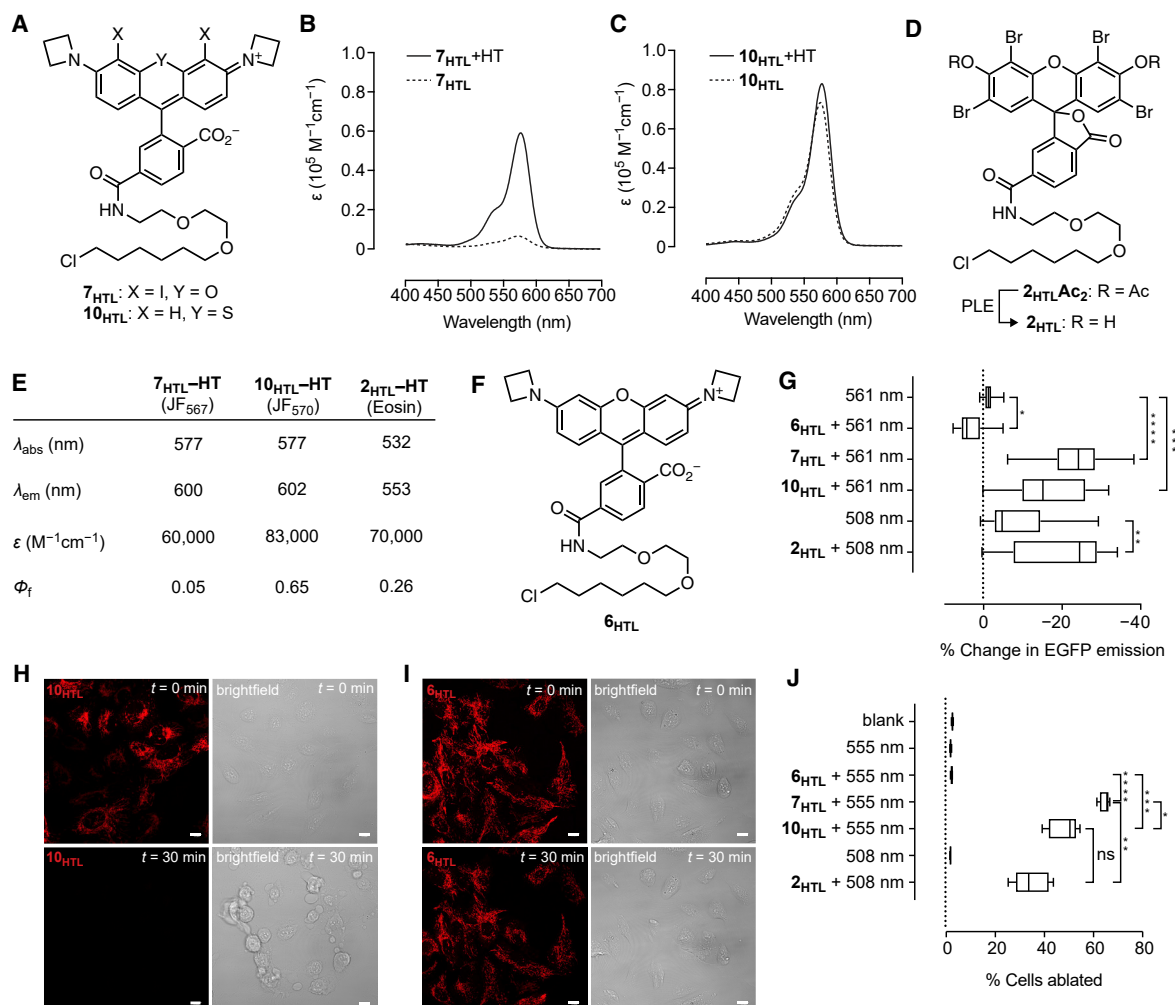
Figure 2. Properties of HaloTag Ligands and Their Utility in CALI and Cell Ablation

(A) Chemical structures of JF_{567}-HaloTag ligand (**7$_{HTL}$**) and JF_{570}-HaloTag ligand (**10$_{HTL}$**).

(B and C) Absorbance spectra of (B) **7$_{HTL}$** and (C) **10$_{HTL}$** ± HaloTag protein (HT).

(D) Chemical structure of eosin-Ac$_2$-HaloTag ligand (**2$_{HTL}$Ac$_2$**) and conversion to **2$_{HTL}$** by incubation with porcine liver esterase (PLE).

(E) Table of photophysical properties for **7$_{HTL}$**, **10$_{HTL}$**, and **2$_{HTL}$** attached to HaloTag protein.

(F) Chemical structure of JF_{549}-HaloTag ligand (**6$_{HTL}$**).

(G) Comparison of EGFP CALI using 561 nm excitation light (laser; 10 W/cm^2) alone (n = 19), 561 nm excitation light (laser; 10 W/cm^2) with **6$_{HTL}$** (n = 15), **7$_{HTL}$** (n = 23), and **10$_{HTL}$** (n = 14), 508-nm centered excitation light (LED; 10 W/cm^2) alone (n = 35), or 508-nm centered excitation light (LED; 10 W/cm^2) with **2$_{HTL}$** (n = 30); center line indicates median; box limits indicate upper and lower quartiles; whiskers indicate min-max; data pooled from two experiments and analyzed via Kruskal-Wallis test with Steel-Dwass-Critchlow-Fligner post-hoc test.

(H and I) Representative confocal fluorescence (561 nm laser excitation) and bright-field microscopy images of U2OS cells expressing HaloTag-TOMM20 fusion protein incubated with JF_{570}-HaloTag ligand (**10$_{HTL}$**) (H) or JF_{549}-HaloTag ligand (**6$_{HTL}$**) (I) before (t = 0 min) and after (t = 30 min) wide-field irradiation with 560-nm centered light. Scale bars, 13 μm.

(J) Comparison of cell ablation efficacy using **6$_{HTL}$**, **7$_{HTL}$**, and **10$_{HTL}$** with 555 nm excitation light or **2$_{HTL}$** using 508-nm centered excitation light in U2OS cells stably expressing HaloTag-TOMM20 fusion protein exposed to 55 mW/cm^2 excitation light for 3 min; center line indicates median; box limits indicate upper and lower quartiles; whiskers indicate min-max; data analyzed via Welch's ANOVA and Games-Howell post-hoc test (n = 5, 10.89 mm^2 microplate wells); n = 5 except for blank measurement where n = 10.

Statistical significance in (G and J) reported as follows: *p < 0.05, **p < 0.01, ***p < 0.001, ****p < 0.0001. See also Figures S1–S3

(**10$_{HTL}$**) showed similar Φ_f values to the free dyes (**7** and **10**) with a slight bathochromic shift of 8–12 nm due to attachment of the HaloTag ligand moiety and conjugation to the HaloTag protein (Figures 1C–1E , 2E, S2B, and S2C). Both dyes exhibited a substantial bathochromic shift (~45 nm) compared with the conjugate of the eosin-HaloTag ligand (**2$_{HTL}$**, Figures 2E and S2D)

and therefore constitute the most red-shifted HaloTag-compatible photosensitizers described.

For an initial application, we tested these photosensitizers in CALI of proteins in live cells. CALI allows the targeted inactivation of proteins via excitation of a conjugated photosensitizer, which produces damaging oxidants, typically singlet oxygen

($^1O_2$) or other radical products such as superoxide (Baptista et al., 2017; Jay, 1988; Liao et al., 1994; Ochsner, 1997). These reactive species act with an effective radius of 4–6 nm (Beck et al., 2002; Linden et al., 1992) via methionine oxidation and protein crosslinking (Yan et al., 2006). Unlike conventional genetic knockout methods, the CALI technique gives temporal control of protein ablation, which may allow for functional knockouts of vital proteins (Vitriol et al., 2007; Wojtovich et al., 2016) with faster time resolution compared with RNAi (Li et al., 2018). CALI has been found useful in studying mitochondrial electron transport chain physiology (Wojtovich et al., 2016) and memory maintenance (Takemoto et al., 2017), making bioavailable and targetable photosensitizers of particular interest in various areas of biology.

For a proof-of-concept CALI experiment, we expressed EGFP-HaloTag fusion proteins in U2OS cells and then labeled with photosensitizer ligands JF$_{567}$-HaloTag ligand (**7$_{HTL}$**), JF$_{570}$-HaloTag ligand (**10$_{HTL}$**), and eosin-Ac$_2$-HaloTag ligand (**2$_{HTL}$Ac$_2$**), with the JF$_{549}$-HaloTag ligand (**6$_{HTL}$**; Figure 2F) and vehicle-only (DMSO) as controls (Figure 2G). CALI efficacy was assessed by measuring the decrease in EGFP fluorescence upon illumination of the cells with photosensitizer excitation light; we chose 561 nm for the JF ligands and 508 nm for the eosin ligand to give comparable absorption cross-sections (Figure S3A). JF$_{567}$-HaloTag ligand (**7$_{HTL}$**) and JF$_{570}$-HaloTag ligand (**10$_{HTL}$**) both showed effective CALI, showing a decrease in EGFP fluorescence after brief photosensitizer excitation (10 s, 561 nm, 10 W/cm^2). Interestingly, cells labeled with JF$_{549}$-HaloTag ligand (**6$_{HTL}$**) showed a small but significant *increase* in average fluorescence intensity under the same conditions, possibly due to the diminutive amount of generated ROS promoting further maturation of EGFP chromophores. CALI experiments with the eosin ligand (**2$_{HTL}$Ac$_2$**) were more complicated due to the overlap of the EGFP and eosin absorbance spectra. Cells labeled with **2$_{HTL}$Ac$_2$** and excited with 508-nm centered light elicited a significant decrease in EGFP fluorescence, but the dye-free control experiment also showed significant bleaching of EGFP by the 508-nm centered light dose. These data demonstrate that both iodination and sulfur substitution yield photosensitizer JF dyes that perform similarly to an established compound in CALI applications. This experiment also showcases the longer absorbance maxima of **7$_{HTL}$** and **10$_{HTL}$**, which could allow concurrent use of these compounds with GFP-based reporters or blue light-excited optogenetic reagents.

Targeted Cell Ablation in Cell Culture

Photosensitizers can also be utilized to ablate entire cells (Miller and Selverston, 1979), presumably via CALI of vital biomolecules or oxidative damage to organelles. Reported targets for effective cell ablation include the nucleus and mitochondria (He et al., 2016; Shirmanova et al., 2015). For nuclear-targeted photosensitization, the hypothesized mechanisms of ablation include DNA damage leading to death of irradiated cells. For mitochondrial-targeted photosensitizers, cell death is presumably caused by mitochondrial membrane damage and subsequent cytochrome *c* leakage leading to apoptosis or decreased energy output potential leading to necrosis. Photoablation of cells can be utilized for clinical applications such as photodynamic therapy of malignancies (Zhang et al., 2018), photoinactivation of

pathogenic microbes (Hu et al., 2018; Wang et al., 2017), or for basic science experiments to study the effect of the ablation of specific cell lineages on animal development or behavior.

We first tested the ablative utility of the JF dyes in cell culture, targeting the HaloTag ligands to the nucleus or mitochondria using HaloTag fusions to either histone H2B ("HaloTag-H2B") or the mitochondrial outer membrane import protein TOMM20 ("HaloTag-TOMM20"). We found that both JF$_{567}$-HaloTag ligand (**7$_{HTL}$**) and JF$_{570}$-HaloTag ligand (**10$_{HTL}$**) were effective ablative agents of U2OS cells stably expressing HaloTag-H2B when excited with 555-nm centered light (3 min, 55 mW/cm^2; Figure S3B), ablating 35% and 19% of cells, respectively, when measured 24 h after illumination. This was better or equivalent to the eosin-Ac$_2$-HaloTag ligand (**2$_{HTL}$Ac$_2$**; 16% ablation; 3 min, 55 mW/cm^2, 508-nm centered light) and substantially larger than the JF$_{549}$-HaloTag ligand (**9**) or DMSO controls, which both showed ~1% ablation under the same illumination conditions (Figure S3C). Similar trends were observed with HaloTag-TOMM20-expressing cells but at higher overall efficacy with JF$_{567}$-HaloTag (**7$_{HTL}$**), JF$_{570}$-HaloTag ligand (**10$_{HTL}$**), and eosin-Ac$_2$-HaloTag ligand (**2$_{HTL}$Ac$_2$**), showing ablation of 65%, 48%, and 35% of cells, respectively, compared with ~2% in the JF$_{549}$-HaloTag ligand (**6$_{HTL}$**) and DMSO-only controls (Figures 2H–2J and S3D). Increasing illumination intensity (147 mW/cm^2) resulted in >80% ablation for both the experiments using the Janelia Fluor photosensitizer HaloTag ligands (Figures S3E and S3F). These compounds also showed negligible "dark" toxicity, demonstrating that the cellular ablation is light mediated (Figures S3G–S3H). Ablation was also negligible in the absence of HaloTag fusion proteins, demonstrating that damage due to nonspecifically bound dyes is nominal (Figure S3I).

Targeted Cell Ablation *In Vivo*

We then tested the utility of this cell ablation strategy *in vivo* using the zebrafish model system. Transgenic casper zebrafish (*Mitfa*$^{w2/w2}$ *roy*$^{a9/a9}$) embryos expressing a neuron-specific *elavl3* GAL4-VP16 driver were injected with a construct resulting in the co-expression of mCerulean3 fluorescent protein and the mitochondria-targeted HaloTag-TOMM20 fusion (Figure 3A). These neurons were labeled with JF$_{570}$-HaloTag ligand (**10$_{HTL}$**) or the previously described bioavailable JF$_{585}$-HaloTag ligand (**20$_{HTL}$**; Figure S4A) (Grimm et al., 2017b) by incubation of these transgenic larval fish with these ligands in the system water (33 μM). Attempts to use **7$_{HTL}$** *in vivo* resulted in poor labeling (data not shown), likely due to the lipophilic iodo substituents combined with the shift in K_{L-Z} toward the lactone form. Both **10$_{HTL}$** and **20$_{HTL}$** dyes labeled neurons throughout the zebrafish brain. We then illuminated the approximate forebrain region (zone 1, Figure 3B) of fish labeled with **10$_{HTL}$** with 3 W/cm^2 and fish incubated with **20$_{HTL}$** with 12 W/cm^2; the higher illumination power used for the JF$_{585}$ accounts for the differences in absorption coefficients at 560-nm centered light. We measured cell viability by counting cells using the mCerulean3 fluorescence signal, finding that, in zone 1 (~forebrain) of JF$_{570}$-labeled fish, only ~3% of cells were viable 24 h post-illumination, whereas use of the JF$_{585}$-HaloTag ligand preserved 93% of the neurons in fish (Figures 3C and 3D). Neuronal viability was also quantified in zones roughly corresponding to the midbrain and hindbrain regions
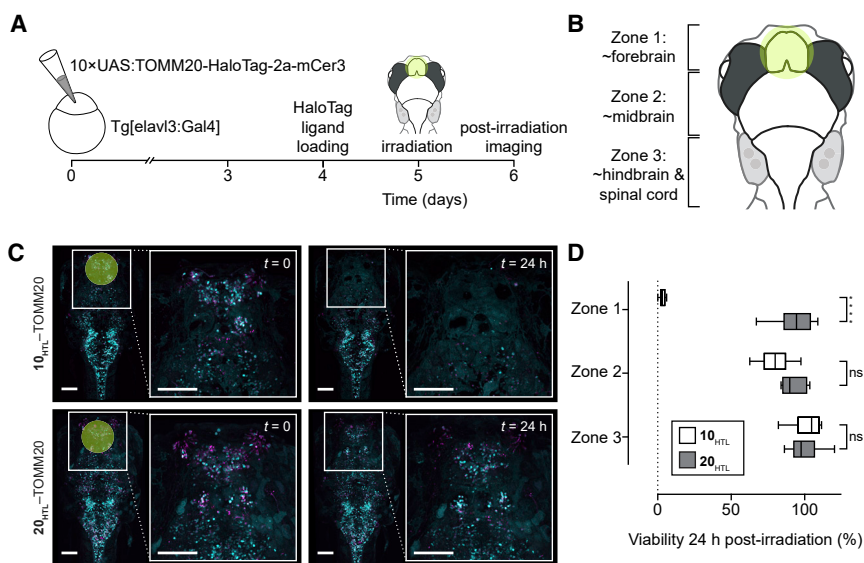
Figure 3. Photoablation of Neurons in Larval Zebrafish

(A) Experimental scheme of larval zebrafish neuronal ablation experiment.

(B) Cartoon of larval zebrafish brain "zones" used in this experiment; yellow circle indicates approximate area of irradiation.

(C) Representative fluorescence microscopy images of zebrafish pre-irradiation ($t = 0$ min), and one day post-irradiation ($t = 24$ h) expressing HaloTag fusions to the mitochondrial protein TOMM20 (magenta) co-expressing mCerulean (cyan) and incubated with either JF$_{570}$-HaloTag ligand (**10$_{HTL}$**, top; 3 W/cm^2 excitation) or JF$_{585}$-HaloTag ligand (**20$_{HTL}$**, bottom; 12 W/cm^2). Scale bars, 100 μm.

(D) Quantification of cell ablation efficacy using JF$_{570}$-HaloTag ligand (**10$_{HTL}$**) with JF$_{585}$-HaloTag ligand (**20$_{HTL}$**) as control; n = 6 for **10$_{HTL}$** experiments and n = 5 for **20$_{HTL}$** experiments; center line indicates median; box limits indicate upper and lower quartiles; whiskers indicate min-max; data analyzed via independent t tests.

Statistical significance reported as follows: *$p < 0.05$, **$p < 0.01$, ***$p < 0.001$, ****$p < 0.0001$. See also Figure S4.

(zones 2 and 3, Figures 3B, S4B, and S4C) to assess off-target ablation due to light scattering (Dobrucki et al., 2007) or damage to neuronal processes projecting into the area of illumination. This off-target ablation was modest in zone 2, with **10$_{HTL}$** zebrafish retaining 80% of labeled cells, and negligible in zone 3, which showed no significant ablation (Figure 3D), indicating that cell death is largely contained to the area of illumination.

DAB Photopolymerization for EM

Finally, we tested the JF photosensitizers as agents for DAB polymerization, which results in the generation of a visibly opaque, osmophilic material. This polymer is an effective contrast agent in both light microscopy and EM. Photosensitizing fluorescent dyes have a rich history in both EM and correlative light microscopy and EM (Deerinck et al., 1994; Gaietta et al., 2002; Grabenbauer et al., 2005; Hoffmann et al., 2010; Liss et al., 2015; Shu et al., 2011), and this photopolymerization complements peroxide-mediated DAB deposition using horseradish peroxidase (Hopkins et al., 2000) and APEX (Lam et al., 2015; Martell et al., 2012). The hybrid system comprised by the photosensitizer Janelia Fluor ligands and the HaloTag combines the modularity and performance of small-molecule photosensitizers, such as eosin (Deerinck et al., 1994), with the genetic specificity of protein-based reagents, such as miniSOG (Shu et al., 2011), but with longer excitation wavelengths. We expressed HaloTag-H2B fusions in human osteosarcoma cells, labeled with either JF$_{567}$-HaloTag ligand (**7$_{HTL}$**) or JF$_{570}$-HaloTag ligand (**10$_{HTL}$**), fixed the cells, imaged them by light microscopy, performed DAB photopolymerization and osmium tetroxide treatment, and then imaged the sample using transmission electron microscopy (TEM). Photooxidation of DAB was specific to cells expressing HaloTag-H2B fusion proteins, and this labeling strategy enabled high-resolution EM in the nucleus (Figures 4A–4D). Histones could be visualized as electron-dense puncta in TEM images and the use of tomographic techniques enabled 3D EM with resolution approaching the

chromatin-nucleosome interface scale (5–24 nm; Figures 4E–4H) (Ou et al., 2017).

DISCUSSION

Light-driven chemical reactions allow the manipulation of biological systems with high spatiotemporal control. Photosensitizers generate ROS, which can be harnessed in a variety of applications ranging from inactivation of individual proteins to the synthesis of imaging contrast agents *in situ*. We transformed the cell-permeable Janelia Fluor scaffold into a photosensitizer system through rational design. The resulting dyes JF$_{567}$ (**7**) and JF$_{570}$ (**10**) show comparable Φ_{SO} values with classic photosensitizers (Figure 1). Their HaloTag ligand derivatives **7$_{HTL}$** and **10$_{HTL}$** are as effective as the established eosin ligand (**2$_{HTL}$**) in CALI and cell culture ablation experiments but are red shifted and can be introduced into biological systems without the use of esterase-sensitive masking groups (Figure 2). This bioavailability of **10** allows extension of this compound's utility to *in vivo* experiments (Figure 3). Both dyes can also be utilized to photopolymerize DAB and show utility in high-resolution EM (Figure 4). Although JF$_{567}$ (**7**) exhibits a substantially higher Φ_{SO} than JF$_{570}$ (**10**, Figure 1E) *in vitro*, the performance of **7$_{HTL}$** in CALI (Figure 2G) and cell ablation in culture (Figure 2J) was only modestly better than **10$_{HTL}$**; both dyes gave comparable DAB photodeposition (Figures 4A–4D). These results, combined with the utility *in vivo* (Figure 3), recommend JF$_{570}$ (**10**) as a general-purpose photosensitizer, with JF$_{567}$ (**7**) reserved for applications that require high amounts of $^1O_2$. Having established these photosensitizing modifications to the core Janelia Fluor rhodamine scaffold, we can combine them into a single compound, apply them to other rhodamine variants, and then further fine-tune these dyes to improve bioavailability and modulate their spectral properties (Grimm et al., 2015, 2017b). Such chemical tools will enable sophisticated cell ablation experiments *in vivo* and advanced imaging experiments such as correlated light microscopy and EM.
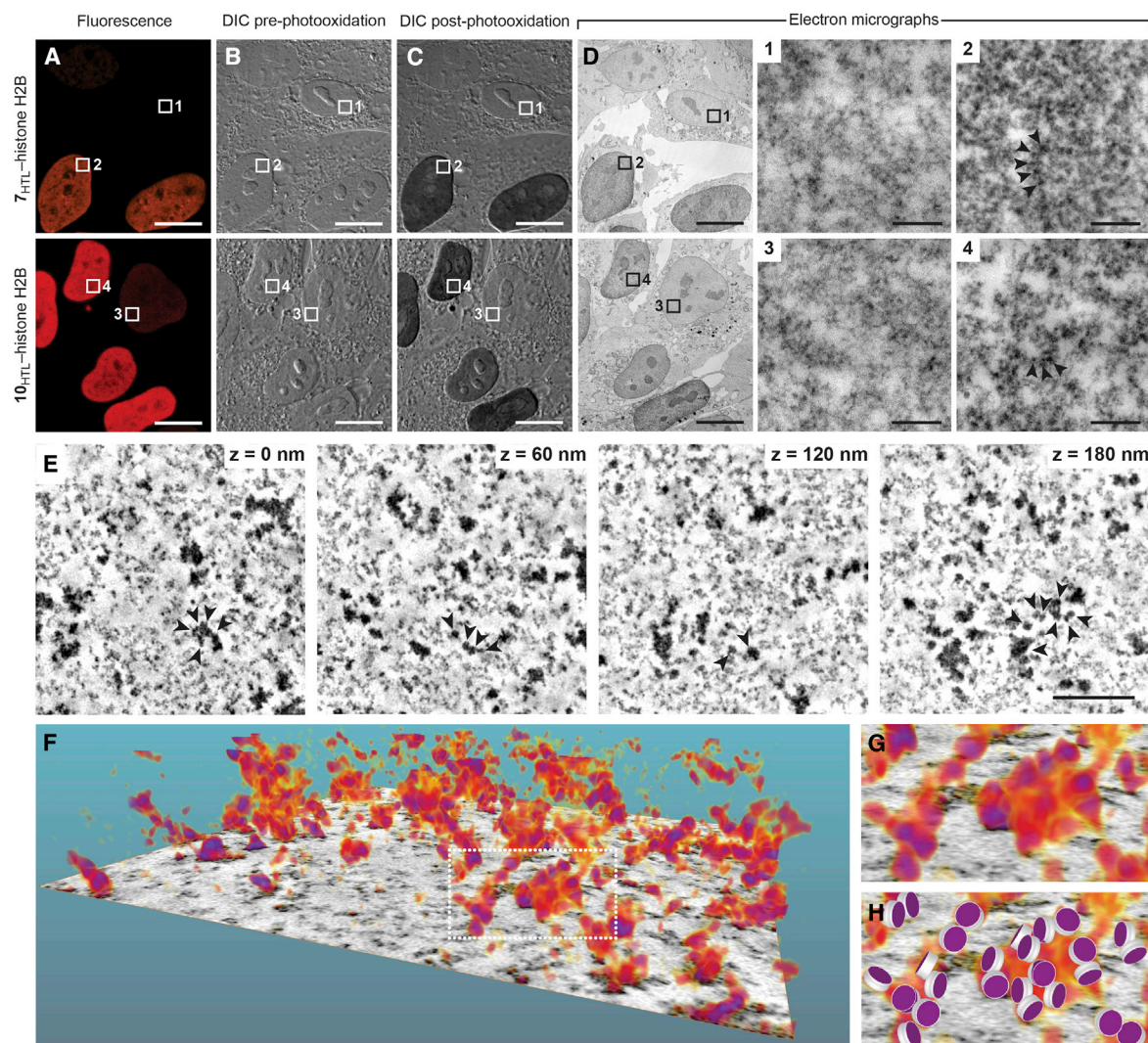
Figure 4. Photooxidation of DAB and EM

(A–D) Representative images of human osteosarcoma (HOS) cells expressing HaloTag-H2B fusion protein labeled with JF$_{567}$-HaloTag ligand (**7$_{HTL}$**; top) or JF$_{570}$-HaloTag ligand (**10$_{HTL}$**, bottom). (A) Pre-photooxidation fluorescence microscopy images. (B) Pre-photooxidation differential interference contrast (DIC) light microscopy images. (C) Post-photooxidation DIC light microscopy images. (D) TEM images post-photooxidation and OsO$_4$ treatment of the entire field of view and regions of interest (ROIs) **1–4**. ROIs **1** and **3** are from cells with low HaloTag-H2B expression and show low staining from DAB photooxidation and OsO$_4$ treatment. ROIs **2** and **4** show increased electron density of the chromatin resulting from specific labeling of **7$_{HTL}$** or **10$_{HTL}$** and subsequent photooxidation of DAB and osmification; arrows highlight representative HaloTag-H2B-containing nucleosomes. Scale bars, 10 μm (A–D) and 200 nm (ROIs **1–4**).

(E) Representative electron tomogram slices in the nucleus of an HOS cell expressing HaloTag-H2B fusion proteins labeled with **10$_{HTL}$**, followed by photo-oxidization of DAB and osmification (cf. ROI **4**). Arrows denote a cluster of nucleosomes in the volume. Scale bar, 200 nm.

(F) 3D volumetric rendering extracted from the electron tomogram in (E).

(G) Magnified view at the segmented chromatin denoted in (F).

(H) Manual matching of stained nucleosomes in (G) with a simplified nucleosome structure consisting of a disc of 11 nm diameter and 5.5 nm height. These imaging experiments were duplicated with similar results.

SIGNIFICANCE

We report the rational design of photosensitizers derived from the azetidine-containing Janelia Fluor rhodamine scaffold. For use in biological systems, we synthesize their HaloTag ligand variants and demonstrate the utility of these compounds in disparate applications. Compared with commercially available photosensitizer HaloTag ligands, these compounds exhibit a bathochromic shift in absorption spectra, allowing illumination with less phototoxic wavelengths of light or multiplexing with fluorescent proteins or optogenetic reagents. These compounds also diffuse in and out of cells and tissue without the need for chemical modification, making use of these chemical tools straightforward. These molecules can be used in a variety of biological experiments, such as destroying individual proteins with

high spatiotemporal control, ablating genetically defined cells in a developing or learning animal, or providing multimodal contrast in light and electron microscopy.

STAR★METHODS

Detailed methods are provided in the online version of this paper and include the following:

- KEY RESOURCES TABLE
- RESOURCE AVAILABILITY
  - ○ Lead Contact
  - ○ Materials Availability
  - ○ Data and Code Availability
- EXPERIMENTAL MODEL AND SUBJECT DETAILS
- METHOD DETAILS
  - ○ General Chemical Synthesis Details
  - ○ Spectroscopy
  - ○ HaloTag Protein Purification
  - ○ Singlet Oxygen Quantum Yield
  - ○ Chromophore Assisted Light Inactivation (CALI) of EGFP in Live Cells
  - ○ Photoablation of Cells in Culture
  - ○ Cloning of Zebrafish Ablation Construct
  - ○ *In Vivo* Ablation of Zebrafish Neurons
  - ○ DAB Photopolymerization for Electron Microscopy
  - ○ EM Sample Preparation and Imaging
- QUANTIFICATION AND STATISTICAL ANALYSES

SUPPLEMENTAL INFORMATION

Supplemental Information can be found online at https://doi.org/10.1016/j.chembiol.2020.07.001.

AUTHOR CONTRIBUTIONS

Conceptualization, T.C.B., J.B.G., Z.L., S.R.A., and L.D.L.; Methodology, T.C.B., A.X.A., J.B.G., A.N.T., G.A.C., S.P., T.A.B., Z.L., S.R.A., M.K., and L.D.L.; Investigation, T.C.B., A.X.A., J.B.G., A.N.T., G.A.C., S.P., L.Z., T.A.B., S.R.A., and M.K.; Formal Analysis, T.C.B., J.B.G., A.N.T., G.A.C., S.R.A., and M.K.; Writing – Original Draft, T.C.B. and L.D.L.; Writing – Review & Editing, T.C.B. and L.D.L.; Visualization, T.C.B., J.B.G., G.A.C., M.K., and L.D.L.; Supervision, T.A.B., Z.L., S.R.A., M.H.E., M.K., and L.D.L.; Project Administration, T.C.B., Z.L., and L.D.L.

DECLARATIONS OF INTERESTS

US Patent 9,933,417 and patent applications US 2019/0367736 and US 2019/0106573 describing azetidine-containing fluorophores and variant composi-tions (with inventors J.B.G. and L.D.L.) are assigned to HHMI. L.D.L. serves on the editorial board of *Cell Chemical Biology*. The authors declare no other competing interests.

REFERENCES

Abdelfattah, A.S., Kawashima, T., Singh, A., Novak, O., Liu, H., Shuai, Y., Huang, Y.C., Campagnola, L., Seeman, S.C., Yu, J., et al. (2019). Bright and photostable chemigenetic indicators for extended in vivo voltage imaging. Science *365*, 699–704.

Ayele, T.M., Knutson, S.D., Ellipilli, S., Hwang, H., and Heemstra, J.M. (2019). Fluorogenic photoaffinity labeling of proteins in living cells. Bioconjug. Chem. *30*, 1309–1313.

Baptista, M.S., Cadet, J., Di Mascio, P., Ghogare, A.A., Greer, A., Hamblin, M.R., Lorente, C., Nunez, S.C., Ribeiro, M.S., Thomas, A.H., et al. (2017). Type I and type II photosensitized oxidation reactions: guidelines and mechanistic pathways. Photochem. Photobiol. *93*, 912–919.

Beck, S., Sakurai, T., Eustace, B.K., Beste, G., Schier, R., Rudert, F., and Jay, D.G. (2002). Fluorophore-assisted light inactivation: a high-throughput tool for direct target validation of proteins. Proteomics *2*, 247–255.

Becker, R.S., Chakravorti, S., and Das, S. (1990). The photosensitizers benzophenoxazine and thiazines: comprehensive investigation of photophysical and photochemical properties. Photochem. Photobiol. *51*, 533–538.

Bulina, M.E., Chudakov, D.M., Britanova, O.V., Yanushevich, Y.G., Staroverov, D.B., Chepurnykh, T.V., Merzlyak, E.M., Shkrob, M.A., Lukyanov, S., and Lukyanov, K.A. (2006). A genetically encoded photosensitizer. Nat. Biotechnol. *24*, 95–99.

Chen, J., Zhang, Z., Li, L., Chen, B.C., Revyakin, A., Hajj, B., Legant, W., Dahan, M., Lionnet, T., Betzig, E., et al. (2014). Single-molecule dynamics of enhanceosome assembly in embryonic stem cells. Cell *156*, 1274–1285.

Chong, S., Dugast-Darzacq, C., Liu, Z., Dong, P., Dailey, G.M., Cattoglio, C., Heckert, A., Banala, S., Lavis, L., Darzacq, X., et al. (2018). Imaging dynamic and selective low-complexity domain interactions that control gene transcription. Science *361*, eaar2555.

de Rosny, E., and Carpentier, P. (2012). GFP-like phototransformation mechanisms in the cytotoxic fluorescent protein KillerRed unraveled by structural and spectroscopic investigations. J. Am. Chem. Soc. *134*, 18015–18021.

Deerinck, T.J., Martone, M.E., Lev-Ram, V., Green, D.P., Tsien, R.Y., Spector, D.L., Huang, S., and Ellisman, M.H. (1994). Fluorescence photooxidation with eosin: a method for high resolution immunolocalization and in situ hybridization detection for light and electron microscopy. J. Cell Biol. *126*, 901–910.

Dobrucki, J.W., Feret, D., and Noatynska, A. (2007). Scattering of exciting light by live cells in fluorescence confocal imaging: phototoxic effects and relevance for FRAP studies. Biophys. J. *93*, 1778–1786.

Douthwright, S., and Sluder, G. (2017). Live cell imaging: assessing the phototoxicity of 488 and 546 nm light and methods to alleviate it. J. Cell Physiol. *232*, 2461–2468.

Ebner, M., Lučić, I., Leonard, T.A., and Yudushkin, I. (2017). PI(3,4,5)P(3) engagement restricts Akt activity to cellular membranes. Mol. Cell *65*, 416–431.e16.

Ezquerra Riega, S.D., Rodriguez, H.B., and San Roman, E. (2017). Rose Bengal in poly(2-hydroxyethyl methacrylate) thin films: self-quenching by photoactive energy traps. Methods Appl. Fluoresc. *5*, 014010.

Fleming, G.R., Knight, A.W.E., Morris, J.M., Morrison, R.J.S., and Robinson, G.W. (1977). Picosecond fluorescence studies of xanthene dyes. J. Am. Chem. Soc. *99*, 4306–4311.

Francisco, C.M.L., Gonçalves, J.M.L.A., Brum, B.S., Santos, T.P.C., Lino-dos-Santos-Franco, A., Silva, D.F.T., and Pavani, C. (2017). The photodynamic efficiency of phenothiazinium dyes is aggregation dependent. New J. Chem. *41*, 14438–14443.

Gaietta, G., Deerinck, T.J., Adams, S.R., Bouwer, J., Tour, O., Laird, D.W., Sosinsky, G.E., Tsien, R.Y., and Ellisman, M.H. (2002). Multicolor and electron microscopic imaging of connexin trafficking. Science *296*, 503–507.

Gandin, E., Lion, Y., and Van de Vorst, A. (1983). Quantum yield of singlet oxygen production by xanthene derivatives. Photochem. Photobiol. *37*, 271–278.

Gold, V. (1987). Compendium of Chemical Terminology: IUPAC Recommendations (Blackwell Scientific Publications).

Grabenbauer, M., Geerts, W.J., Fernandez-Rodriguez, J., Hoenger, A., Koster, A.J., and Nilsson, T. (2005). Correlative microscopy and electron tomography of GFP through photooxidation. Nat. Methods *2*, 857–862.

Grimm, J.B., English, B.P., Chen, J., Slaughter, J.P., Zhang, Z., Revyakin, A., Patel, R., Macklin, J.J., Normanno, D., Singer, R.H., et al. (2015). A general method to improve fluorophores for live-cell and single-molecule microscopy. Nat. Methods *12*, 244–250.

Grimm, J.B., Brown, T.A., Tkachuk, A.N., and Lavis, L.D. (2017a). General synthetic method for Si-fluoresceins and Si-rhodamines. ACS Cent. Sci. *3*, 975–985.

Grimm, J.B., Muthusamy, A.K., Liang, Y., Brown, T.A., Lemon, W.C., Patel, R., Lu, R., Macklin, J.J., Keller, P.J., Ji, N., et al. (2017b). A general method to fine-tune fluorophores for live-cell and in vivo imaging. Nat. Methods *14*, 987–994.

Grzegorski, S.J., Chiari, E.F., Robbins, A., Kish, P.E., and Kahana, A. (2014). Natural variability of Kozak sequences correlates with function in a zebrafish model. PLoS One *9*, e108475.

He, J., Wang, Y., Missinato, M.A., Onuoha, E., Perkins, L.A., Watkins, S.C., St Croix, C.M., Tsang, M., and Bruchez, M.P. (2016). A genetically targetable near-infrared photosensitizer. Nat. Methods *13*, 263–268.

Hoffmann, C., Gaietta, G., Zurn, A., Adams, S.R., Terrillon, S., Ellisman, M.H., Tsien, R.Y., and Lohse, M.J. (2010). Fluorescent labeling of tetracysteine-tagged proteins in intact cells. Nat. Protoc. *5*, 1666–1677.

Hopkins, C., Gibson, A., Stinchcombe, J., and Futter, C. (2000). Chimeric molecules employing horseradish peroxidase as reporter enzyme for protein localization in the electron microscope. Methods Enzymol. *327*, 35–45.

Hu, X., Huang, Y.Y., Wang, Y., Wang, X., and Hamblin, M.R. (2018). Antimicrobial photodynamic therapy to control clinically relevant biofilm infections. Front. Microbiol. *9*, 1299.

Jay, D.G. (1988). Selective destruction of protein function by chromophore-assisted laser inactivation. Proc. Natl. Acad. Sci. U S A *85*, 5454–5458.

Kimura, Y., Satou, C., and Higashijima, S. (2008). V2a and V2b neurons are generated by the final divisions of pair-producing progenitors in the zebrafish spinal cord. Development *135*, 3001–3005.

Kwan, K.M., Fujimoto, E., Grabher, C., Mangum, B.D., Hardy, M.E., Campbell, D.S., Parant, J.M., Yost, H.J., Kanki, J.P., and Chien, C.B. (2007). The Tol2kit: a multisite gateway-based construction kit for Tol2 transposon transgenesis constructs. Dev. Dyn. *236*, 3088–3099.

Lam, S.S., Martell, J.D., Kamer, K.J., Deerinck, T.J., Ellisman, M.H., Mootha, V.K., and Ting, A.Y. (2015). Directed evolution of APEX2 for electron microscopy and proximity labeling. Nat. Methods *12*, 51–54.

Lavis, L.D., Chao, T.Y., and Raines, R.T. (2006). Fluorogenic label for biomolecular imaging. ACS Chem. Biol. *1*, 252–260.

Lavis, L.D., Chao, T.Y., and Raines, R.T. (2011). Synthesis and utility of fluorogenic acetoxymethyl ethers. Chem. Sci. *2*, 521–530.

Lawrence, A., Bouwer, J.C., Perkins, G., and Ellisman, M.H. (2006). Transform-based backprojection for volume reconstruction of large format electron microscope tilt series. J. Struct. Biol. *154*, 144–167.

Lee, J., Yu, P., Xiao, X., and Kodadek, T. (2008). A general system for evaluating the efficiency of chromophore-assisted light inactivation (CALI) of proteins reveals Ru(II) tris-bipyridyl as an unusually efficient "warhead". Mol. Biosyst. *4*, 59–65.

Li, Y., Aggarwal, M.B., Ke, K., Nguyen, K., and Spitale, R.C. (2018). Improved analysis of RNA localization by spatially restricted oxidation of RNA-protein complexes. Biochemistry *57*, 1577–1581.

Liao, J.C., Roider, J., and Jay, D.G. (1994). Chromophore-assisted laser inactivation of proteins is mediated by the photogeneration of free radicals. Proc. Natl. Acad. Sci. U S A *91*, 2659–2663.

Linden, K.G., Liao, J.C., and Jay, D.G. (1992). Spatial specificity of chromophore assisted laser inactivation of protein function. Biophys. J. *61*, 956–962.

Liss, V., Barlag, B., Nietschke, M., and Hensel, M. (2015). Self-labelling enzymes as universal tags for fluorescence microscopy, super-resolution microscopy and electron microscopy. Sci. Rep. *5*, 17740.

Lo, C.A., Kays, I., Emran, F., Lin, T.J., Cvetkovska, V., and Chen, B.E. (2015). Quantification of protein levels in single living cells. Cell Rep. *13*, 2634–2644.

Los, G.V., Encell, L.P., McDougall, M.G., Hartzell, D.D., Karassina, N., Zimprich, C., Wood, M.G., Learish, R., Ohana, R.F., Urh, M., et al. (2008). HaloTag: a novel protein labeling technology for cell imaging and protein analysis. ACS Chem. Biol. *3*, 373–382.

Lukinavicius, G., Umezawa, K., Olivier, N., Honigmann, A., Yang, G., Plass, T., Mueller, V., Reymond, L., Correa, I.R., Jr., Luo, Z.G., et al. (2013). A near-infrared fluorophore for live-cell super-resolution microscopy of cellular proteins. Nat. Chem. *5*, 132–139.

Magidson, V., and Khodjakov, A. (2013). Circumventing photodamage in live-cell microscopy. Methods Cell Biol. *114*, 545–560.

Marek, K.W., and Davis, G.W. (2002). Transgenically encoded protein photo-inactivation (FlAsH-FALI): acute inactivation of synaptotagmin I. Neuron *36*, 805–813.

Markwardt, M.L., Kremers, G.J., Kraft, C.A., Ray, K., Cranfill, P.J., Wilson, K.A., Day, R.N., Wachter, R.M., Davidson, M.W., and Rizzo, M.A. (2011). An improved cerulean fluorescent protein with enhanced brightness and reduced reversible photoswitching. PLoS One *6*, e17896.

Martell, J.D., Deerinck, T.J., Sancak, Y., Poulos, T.L., Mootha, V.K., Sosinsky, G.E., Ellisman, M.H., and Ting, A.Y. (2012). Engineered ascorbate peroxidase as a genetically encoded reporter for electron microscopy. Nat. Biotechnol. *30*, 1143–1148.

Mastronarde, D.N. (1997). Dual-axis tomography: an approach with alignment methods that preserve resolution. J. Struct. Biol. *120*, 343–352.

Miller, J.P., and Selverston, A. (1979). Rapid killing of single neurons by irradiation of intracellularly injected dye. Science *206*, 702–704.

Ochsner, M. (1997). Photophysical and photobiological processes in the photodynamic therapy of tumours. J. Photochem. Photobiol. B *39*, 1–18.

Onukwufor, J.O., Trewin, A.J., Baran, T.M., Almast, A., Foster, T.H., and Wojtovich, A.P. (2020). Quantification of reactive oxygen species production by the red fluorescent proteins KillerRed, SuperNova and mCherry. Free Radic. Biol. Med. *147*, 1–7.

Ou, H.D., Deerinck, T.J., Bushong, E., Ellisman, M.H., and O'Shea, C.C. (2015). Visualizing viral protein structures in cells using genetic probes for correlated light and electron microscopy. Methods *90*, 39–48.

Ou, H.D., Phan, S., Deerinck, T.J., Thor, A., and O'Shea, C.C. (2017). ChromEMT: visualizing 3D chromatin structure and compaction in interphase and mitotic cells. Science *357*, eaag0025.

Pal, P., Zeng, H., Durocher, G., Girard, D., Li, T., Gupta, A.K., Giasson, R., Blanchard, L., Gaboury, L., Balassy, A., et al. (1996). Phototoxicity of some bromine-substituted rhodamine dyes: synthesis, photophysical properties and application as photosensitizers. Photochem. Photobiol. *63*, 161–168.

Phan, S., Boassa, D., Nguyen, P., Wan, X., Lanman, J., Lawrence, A., and Ellisman, M.H. (2017). 3D reconstruction of biological structures: automated procedures for alignment and reconstruction of multiple tilt series in electron tomography. Adv. Struct. Chem. Imaging *2*, 8.

Phan, S., Lawrence, A., Molina, T., Lanman, J., Berlanga, M., Terada, M., Kulungowski, A., Obayashi, J., and Ellisman, M. (2012). TxBR montage reconstruction for large field electron tomography. J. Struct. Biol. *180*, 154–164.

Riani, Y.D., Matsuda, T., Takemoto, K., and Nagai, T. (2018). Green monomeric photosensitizing fluorescent protein for photo-inducible protein inactivation and cell ablation. BMC Biol. *16*, 50.

Ruiz-Gonzalez, R., Cortajarena, A.L., Mejias, S.H., Agut, M., Nonell, S., and Flors, C. (2013). Singlet oxygen generation by the genetically encoded tag miniSOG. J. Am. Chem. Soc. *135*, 9564–9567.

Sawinski, J., Wallace, D.J., Greenberg, D.S., Grossmann, S., Denk, W., and Kerr, J.N. (2009). Visually evoked activity in cortical cells imaged in freely moving animals. Proc. Natl. Acad. Sci. U S A *106*, 19557–19562.

Schindelin, J., Arganda-Carreras, I., Frise, E., Kaynig, V., Longair, M., Pietzsch, T., Preibisch, S., Rueden, C., Saalfeld, S., Schmid, B., et al. (2012). Fiji: an open-source platform for biological-image analysis. Nat. Methods *9*, 676–682.

Seybold, P.G., Gouterman, M., and Callis, J. (1969). Calorimetric, photometric and lifetime determinations of fluorescence yields of fluorescein dyes. Photochem. Photobiol. *9*, 229–242.

Shirmanova, M., Yuzhakova, D., Snopova, L., Perelman, G., Serebrovskaya, E., Lukyanov, K., Turchin, I., Subochev, P., Lukyanov, S., Kamensky, V., et al. (2015). Towards PDT with genetically encoded photosensitizer KillerRed: a comparison of continuous and pulsed laser regimens in an animal tumor model. PLoS One *10*, e0144617.

Shu, X., Lev-Ram, V., Deerinck, T.J., Qi, Y., Ramko, E.B., Davidson, M.W., Jin, Y., Ellisman, M.H., and Tsien, R.Y. (2011). A genetically encoded tag for correlated light and electron microscopy of intact cells, tissues, and organisms. PLoS Biol. *9*, e1001041.

Takemoto, K., Iwanari, H., Tada, H., Suyama, K., Sano, A., Nagai, T., Hamakubo, T., and Takahashi, T. (2017). Optical inactivation of synaptic AMPA receptors erases fear memory. Nat. Biotechnol. *35*, 38–47.

Takemoto, K., Matsuda, T., McDougall, M., Klaubert, D.H., Hasegawa, A., Los, G.V., Wood, K.V., Miyawaki, A., and Nagai, T. (2011). Chromophore-assisted light inactivation of HaloTag fusion proteins labeled with eosin in living cells. ACS Chem. Biol. *6*, 401–406.

Takemoto, K., Matsuda, T., Sakai, N., Fu, D., Noda, M., Uchiyama, S., Kotera, I., Arai, Y., Horiuchi, M., Fukui, K., et al. (2013). SuperNova, a monomeric photosensitizing fluorescent protein for chromophore-assisted light inactivation. Sci. Rep. *3*, 2629.

Torra, J., Lafaye, C., Signor, L., Aumonier, S., Flors, C., Shu, X., Nonell, S., Gotthard, G., and Royant, A. (2019). Tailing miniSOG: structural bases of the complex photophysics of a flavin-binding singlet oxygen photosensitizing protein. Sci. Rep. *9*, 2428.

Tour, O., Meijer, R.M., Zacharias, D.A., Adams, S.R., and Tsien, R.Y. (2003). Genetically targeted chromophore-assisted light inactivation. Nat. Biotechnol. *21*, 1505–1508.

Vitriol, E.A., Uetrecht, A.C., Shen, F., Jacobson, K., and Bear, J.E. (2007). Enhanced EGFP-chromophore-assisted laser inactivation using deficient cells rescued with functional EGFP-fusion proteins. Proc. Natl. Acad. Sci. U S A *104*, 6702–6707.

Wang, Y., Wang, Y., Wang, Y., Murray, C.K., Hamblin, M.R., Hooper, D.C., and Dai, T. (2017). Antimicrobial blue light inactivation of pathogenic microbes: state of the art. Drug Resist. Updat. *33-35*, 1–22.

Wojtovich, A.P., Wei, A.Y., Sherman, T.A., Foster, T.H., and Nehrke, K. (2016). Chromophore-assisted light inactivation of mitochondrial electron transport chain complex II in *Caenorhabditis elegans*. Sci. Rep. *6*, 29695.

Xiong, Y., Tian, X., and Ai, H.W. (2019). Molecular tools to generate reactive oxygen species in biological systems. Bioconjug. Chem. *30*, 1297–1303.

Yan, P., Xiong, Y., Chen, B., Negash, S., Squier, T.C., and Mayer, M.U. (2006). Fluorophore-assisted light inactivation of calmodulin involves singlet-oxygen mediated cross-linking and methionine oxidation. Biochemistry *45*, 4736–4748.

Zhang, J., Jiang, C., Figueiro Longo, J.P., Azevedo, R.B., Zhang, H., and Muehlmann, L.A. (2018). An updated overview on the development of new photosensitizers for anticancer photodynamic therapy. Acta Pharm. Sin. B *8*, 137–146.

Zheng, Q., Ayala, A.X., Chung, I., Weigel, A.V., Ranjan, A., Falco, N., Grimm, J.B., Tkachuk, A.N., Wu, C., Lippincott-Schwartz, J., et al. (2019). Rational design of fluorogenic and spontaneously blinking labels for super-resolution imaging. ACS Cent. Sci. *5*, 1602–1613.

STAR★METHODS

KEY RESOURCES TABLE

REAGENT or RESOURCE	SOURCE	IDENTIFIER
Chemicals, Peptides, and Recombinant Proteins		
Singlet Oxygen Sensor Green	Invitrogen	Thermo Fisher Scientific Catalog #S36002
JF_{567} (**7**)	Janelia Research Campus; this paper	N/A
JF_{567}–HaloTag ligand (**7$_{HTL}$**)	Janelia Research Campus; this paper	N/A
JF_{570} (**10**)	Janelia Research Campus; this paper	N/A
JF_{570}–HaloTag ligand (**10$_{HTL}$**)	Janelia Research Campus; this paper	N/A
Eosin-Ac$_2$–HaloTag ligand (**2$_{HTL}$Ac$_2$**)	Promega	N/A
Eosin Y	Sigma Aldrich	Sigma Aldrich Catalog #E4009
JF_{549} (**6**)	Janelia Research Campus; (Grimm et al., 2015)	N/A
JF_{585}–HaloTag ligand (**20$_{HTL}$**)	Janelia Research Campus; (Grimm et al., 2017b)	N/A
Rose Bengal	Sigma Aldrich	Sigma Aldrich Catalog #330000
JF_{549}–HaloTag ligand (**6$_{HTL}$**)	Janelia Research Campus; (Grimm et al., 2015)	N/A
Porcine liver esterase (PLE)	Sigma Aldrich	Sigma Aldrich Catalog #E3019
NucBlue™ Live ReadyProbes™ Reagent	Invitrogen	Thermo Fisher Scientific Catalog #R37605
NucRed™ Dead 647 ReadyProbes™ Reagent	Invitrogen	Thermo Fisher Scientific Catalog #R37113
Gateway LR Clonase II Enzyme Mix	Invitrogen	Thermo Fisher Scientific Catalog #11791020
Durcupan™ ACM	Sigma Aldrich	Sigma Aldrich Catalog #44610
Experimental Models: Cell Lines		
Human: U2OS cell line	ATCC	RRID: CVCL_0042
Human: U2OS cell line expressing HaloTag-H2B	Janelia Research Campus; ATCC; HT-H2B sequence; (Chen et al., 2014)	Modified cells of RRID: CVCL_0042
Human: U2OS cell line expressing HaloTag-TOMM20	Janelia Research Campus; ATCC; TOMM20 sequence from Michael Davidson, FSU	Modified cells of RRID: CVCL_0042
Human: HOS cell line: HaloTag-Histone H2B (HT-H2B)	UCSD; ATCC	Modified cells of RRID:CVCL_0312
Experimental Models: Organisms/Strains		
Mitfa$^{w2/w2}$ *roy*$^{a9/a9}$ (Casper) zebrafish (Danio rerio), Tg(elavl3:Gal4-VP16)	Janelia Research Campus; (Kimura et al., 2008)	N/A
Recombinant DNA		
pHaloTag-EGFP	Thomas Leonard & Ivan Yudushkin; (Ebner et al., 2017).	http://n2t.net/addgene:86629; RRID:Addgene_86629
pRSET.HaloTag	Janelia Research Campus; pRSET: Invitrogen; HaloTag: Promega	pRSET - V35120; HaloTag - N/A
10xUAS:TOMM20-HaloTagv7-p2a-mCerulean3, myl7:EGFP	Janelia Research Campus; Tol2 destination vector:(Kwan et al., 2007); Kozak sequence: (Grzegorski et al., 2014); Native TOMM20: Accession NM_001002698; NP_001002698); HaloTagv7: Promega; P2A sequence – (Lo et al., 2015); mCerulean3 sequence: (Markwardt et al., 2011).	N/A

REAGENT or RESOURCE	SOURCE	IDENTIFIER
Continued		
Software and Algorithms		
XLSTAT v2020.1.1 add-in to Microsoft Excel 2019 v1908 build 11929.20838	Addinsoft	http://www.xlstat.com/en/
GraphPad Prism 7.04	GraphPad Software	https://www.graphpad.com/scientific-software/prism/
Fiji ImageJ Distribution 2.0.0-rc-69/1.52i	(Schindelin et al., 2012)	https://fiji.sc/
Amira 6.3	Thermo Fisher Scientific	N/A

RESOURCE AVAILABILITY

Lead Contact
Further information and requests for resources and reagents should be directed to and will be fulfilled by the Lead Contact, Luke D. Lavis: lavisl@janelia.hhmi.org.

Materials Availability
Aliquots of JF_{567}–HaloTag ligand (**7**$_{HTL}$) and JF_{570}–HaloTag ligand (**10**$_{HTL}$) are available by request from the Lead Contact.

Data and Code Availability
This study did not generate new datasets or code.

EXPERIMENTAL MODEL AND SUBJECT DETAILS

Cells utilized in CALI and ablation experiments were U2OS cells (human female, osteosarcoma), some with genetic alterations for the expression of various HaloTag fusion proteins: transiently transfected EGFP; stably expressed HaloTag–histone H2B fusions; stably expressed HaloTag–TOMM20 fusions. U2OS cells for CALI experiments were maintained in Dulbecco's Modified Eagle Medium (DMEM; 4.5 g/L glucose and sodium pyruvate, −L-glutamine, −phenol red; Corning) supplemented with 10% (v/v) fetal bovine serum (FBS; Gibco), 2 mM L-glutamine (Gibco), 100 U/mL penicillin and 100 U/mL streptomycin (Gibco), and 5% CO_2 at 37°C. U2OS cells for ablation experiments were maintained in DMEM (high glucose, −glutamine, −phenol red; Gibco) containing 1× GlutaMax (Gibco), 10% v/v FBS (Gibco) and 5% CO_2 at 37°C. 1× Antibiotic–Antimycotic (Gibco) was used for maintenance only (excluded from imaging/treatment formulations) and cells were passaged at approximately 80% confluence with 0.25% Trypsin–EDTA with phenol red (Gibco). Human osteosarcoma (HOS) cells (female) expressing HaloTag–histone H2B fusions utilized for electron microscopy experiments were cultured on 35 mm MatTek dishes (MatTek Corp) in DMEM (Gibco) containing 10% v/v FBS (Gibco) without antibiotic.

Embryonic Casper (*Mitfa*$^{w2/w2}$ *roy*$^{a9/a9}$) zebrafish (*Danio rerio*) were utilized from the 1–2 cell stage through day 6 post-fertilization as detailed below. All zebrafish experiments presented in this study were conducted in accordance with the animal research guidelines from the National Institutes of Health and were approved by the Institutional Animal Care and Use Committee and Institutional Biosafety Committee of Janelia Research Campus.

HaloTag protein expressed by and subsequently purified from BL21 chemically competent *E. coli*.

METHOD DETAILS

General Chemical Synthesis Details
Commercial reagents were obtained from reputable suppliers and used as received. All solvents were purchased in septum-sealed bottles stored under an inert atmosphere. All reactions were sealed with septa through which a nitrogen atmosphere was introduced unless otherwise noted. Reactions were conducted in round-bottomed flasks or septum-capped crimp-top vials containing Teflon-coated magnetic stir bars. Heating of reactions was accomplished with a silicon oil bath or an aluminum reaction block on top of a stirring hotplate equipped with an electronic contact thermometer to maintain the indicated temperatures.

Reactions were monitored by thin layer chromatography (TLC) on precoated TLC glass plates (silica gel 60 F_{254}, 250 μm thickness) or by LC/MS (Phenomenex Kinetex 2.1 mm × 30 mm 2.6 μm C18 column; 5 μL injection; 5–98% MeCN/H_2O, linear gradient, with constant 0.1% v/v HCO_2H additive; 6 min run; 0.5 mL/min flow; ESI; positive ion mode). TLC chromatograms were visualized by UV illumination or developed with *p*-anisaldehyde, ceric ammonium molybdate, or $KMnO_4$ stain. Reaction products were purified by flash chromatography on an automated purification system using pre-packed silica gel columns or by preparative HPLC (Phenomenex Gemini–NX 30 × 150 mm 5 μm C18 column). Analytical HPLC analysis was performed with an Agilent Eclipse XDB 4.6 × 150 mm 5 μm C18 column under the indicated conditions. High-resolution mass spectrometry was performed by the High Resolution Mass Spectrometry Facility at the University of Iowa.

NMR spectra were recorded on a 400 MHz spectrometer. [1]H and ^{13}C chemical shifts were referenced to TMS or residual solvent peaks. Data for ^{1}H NMR spectra are reported as follows: chemical shift (δ ppm), multiplicity (s = singlet, d = doublet, t = triplet, q = quartet, dd = doublet of doublets, m = multiplet), coupling constant (Hz), integration. Data for ^{13}C NMR spectra are reported by chemical shift (δ ppm) with hydrogen multiplicity (C, CH, CH_2, CH_3) information obtained from DEPT spectra.

JF_{567} (7)

JF_{549} (**6**; 500 mg, 1.22 mmol) was taken up in CH_3CN (40 mL), and *N*-iodosuccinimide (1.10 g, 4.87 mmol, 4 eq) was added portionwise over 10 min. After stirring the reaction at room temperature for 3 h, it was concentrated to half volume, diluted with water, and extracted with CH_2Cl_2 (2×). The combined organic extracts were washed with brine, dried over anhydrous $MgSO_4$, filtered, and evaporated. Flash chromatography on silica gel (0–30% EtOAc/toluene) afforded 699 mg (87%) of JF_{567} (**7**) as a purple solid. ^{1}H NMR ($CDCl_3$, 400 MHz) δ 8.00 (dt, *J* = 7.3, 1.1 Hz, 1H), 7.65 (td, *J* = 7.4, 1.3 Hz, 1H), 7.60 (td, *J* = 7.4, 1.2 Hz, 1H), 7.19 – 7.11 (m, 1H), 6.58 (d, *J* = 8.7 Hz, 2H), 6.21 (d, *J* = 8.7 Hz, 2H), 4.24 (q, *J* = 7.4 Hz, 4H), 4.17 (q, *J* = 7.4 Hz, 4H), 2.25 (p, *J* = 7.4 Hz, 4H); ^{13}C NMR ($CDCl_3$, 101 MHz) δ 169.4 (C), 155.2 (C), 153.0 (C), 152.4 (C), 135.0 (CH), 129.8 (CH), 128.2 (CH), 127.2 (C), 125.1 (CH), 124.1 (CH), 110.32 (CH), 110.27 (C), 84.3 (C), 69.1 (C), 54.8 (CH_2), 16.3 (CH_2); Analytical HPLC: t_R = 12.5 min, >99% purity (10–95% MeCN/H_2O, linear gradient, with constant 0.1% v/v TFA additive; 20 min run; 1 mL/min flow; ESI; positive ion mode; detection at 575 nm); HRMS (ESI) calcd for $C_{26}H_{21}I_2N_2O_3$ [M+H]$^+$ 662.9636, found 662.9654.

JF_{567}–HaloTag Ligand (7_{HTL})

6-Carboxy-JF_{549} (**11**; TFA salt; 100 mg, 1.22 mmol) was taken up in CH_3CN (8 mL), and *N*-iodosuccinimide (317 mg, 1.41 mmol, 8 eq) was added. After stirring the reaction at room temperature for 18 h, 1 M NaOH (5 mL) was added. Following 5 min of vigorous stirring, the mixture was acidified with 1 M HCl (5.5 mL), diluted with water, and extracted with 15% *i*-PrOH/$CHCl_3$ (3×). The combined organic extracts were dried over anhydrous $MgSO_4$, filtered, and evaporated. The crude material was purified by reverse phase HPLC (10–75% MeCN/H_2O, linear gradient, with constant 0.1% v/v TFA additive). The pooled HPLC product fractions were partially concentrated to remove MeCN and extracted with 10% MeOH/CH_2Cl_2 (3×). The organic extracts were dried over anhydrous $MgSO_4$, filtered, and evaporated to afford 6-carboxy-JF_{567} (**12**) as a dark purple solid (30 mg, 21%, TFA salt).

6-Carboxy-JF_{567} (**12**; TFA salt; 30 mg, 36.6 μmol) was combined with DSC (22.5 mg, 87.8 μmol, 2.4 eq) in DMF (2 mL). After adding Et_3N (30.6 μL, 219 μmol, 6 eq) and DMAP (0.4 mg, 3.7 μmol, 0.1 eq), the reaction was stirred at room temperature for 1 h. HaloTag(O2) amine (HTL-NH_2, **13**; TFA salt; 37.1 mg, 110 μmol, 3 eq) in DMF (250 μL) was added, and the reaction was stirred an additional 2 h at room temperature. It was subsequently diluted with saturated $NaHCO_3$ and extracted with EtOAc (2×). The combined organic extracts were washed with brine, dried over anhydrous $MgSO_4$, filtered, and concentrated *in vacuo*. The residue was purified by reverse phase HPLC (20–70% MeCN/H_2O, linear gradient, with constant 0.1% v/v TFA additive); pooled HPLC product fractions were partially concentrated to remove MeCN, diluted with saturated $NaHCO_3$, and extracted with CH_2Cl_2 (2×). The organics were dried over anhydrous $MgSO_4$, filtered, and evaporated to afford 18.5 mg (55%) of JF_{567}–HaloTag ligand (7_{HTL}) as a purple solid. ^{1}H NMR ($CDCl_3$, 400 MHz) δ 8.07 – 7.97 (m, 2H), 7.53 – 7.48 (m, 1H), 6.75 (bs, 1H), 6.57 (d, *J* = 8.7 Hz, 2H), 6.21 (d, *J* = 8.7 Hz, 2H), 4.25 (q, *J* = 7.4 Hz, 4H), 4.19 (q, *J* = 7.4 Hz, 4H), 3.66 – 3.57 (m, 6H), 3.55 – 3.48 (m, 4H), 3.37 (t, *J* = 6.6 Hz, 2H), 2.25 (p, *J* = 7.4 Hz, 4H), 1.78 – 1.69 (m, 2H), 1.53 – 1.45 (m, 2H), 1.45 – 1.36 (m, 2H), 1.35 – 1.27 (m, 2H); Analytical HPLC: t_R = 13.1 min, >99% purity (10–95% MeCN/H_2O, linear gradient, with constant 0.1% v/v TFA additive; 20 min run; 1 mL/min flow; ESI; positive ion mode; detection at 575 nm); HRMS (ESI) calcd for $C_{37}H_{41}ClI_2N_3O_6$ [M+H]$^+$ 912.0768, found 912.0782.

Bis(3-bromophenyl)sulfane (16)

An oven-dried round-bottom flask was charged with CuI (604 mg, 3.17 mmol, 0.1 eq) and K_2CO_3 (8.77 g, 63.5 mmol, 2 eq). The flask was sealed and evacuated/backfilled with nitrogen (3×). Isopropanol (125 mL) was added, followed by ethylene glycol (3.54 mL, 63.5 mmol, 2 eq), 3-bromothiophenol (**14**; 3.28 mL, 31.7 mmol), and 3-bromoiodobenzene (**15**; 4.45 mL, 34.9 mmol, 1.1 eq). The reaction mixture was stirred at 80°C for 18 h. It was then diluted with saturated NH_4Cl (200 mL) and EtOAc (200 mL), vigorously stirred for 30 min, and filtered through Celite. The filtrate was separated, and the aqueous layer was extracted again with EtOAc. The combined organics were washed with brine, dried over anhydrous $MgSO_4$, filtered, and evaporated. Flash chromatography (100% hexanes, linear gradient) afforded 8.93 g (82%) of dibromide **16** as a colorless oil. ^{1}H NMR ($CDCl_3$, 400 MHz) δ 7.48 (t, *J* = 1.8 Hz, 2H), 7.40 (ddd, *J* = 7.8, 1.9, 1.2 Hz, 2H), 7.28 – 7.23 (m, 2H), 7.18 (t, *J* = 7.8 Hz, 2H); ^{13}C NMR ($CDCl_3$, 101 MHz) δ 137.3 (C), 133.8 (CH), 130.79 (CH), 130.75 (CH), 129.8 (CH), 123.3 (C); HRMS (EI) calcd for $C_{12}H_8Br_2S$ [M]$^{+\cdot}$ 341.8708, found 341.8732.

Bis(3-(azetidin-1-yl)phenyl)sulfane (17)

An oven-dried round-bottom flask was charged with CuI (985 mg, 5.17 mmol, 0.2 eq), L-proline (1.19 g, 10.4 mmol, 0.4 eq), and K_2CO_3 (14.30 g, 103.5 mmol, 4 eq). The flask was sealed and evacuated/backfilled with nitrogen (3×). A solution of dibromide **16** (8.90 g, 25.9 mmol) in DMSO (100 mL) was added, and the reaction was flushed again with nitrogen (3×). Following the addition of azetidine (10.46 mL, 155.2 mmol, 6 eq), the reaction was stirred at 100°C for 18 h. It was then cooled to room temperature, diluted with saturated NH_4Cl, and extracted with EtOAc (2×). The combined organic extracts were washed with water and brine, dried over anhydrous $MgSO_4$, filtered, and concentrated *in vacuo*. Purification by flash chromatography on silica gel (0–30% EtOAc/hexanes, linear gradient) afforded **17** (6.08 g, 79%) as a white solid. ^{1}H NMR ($CDCl_3$, 400 MHz) δ 7.11 (t, *J* = 7.9 Hz, 2H), 6.68 (ddd, *J* = 7.7, 1.7, 1.0 Hz, 2H), 6.45 (t, *J* = 2.0 Hz, 2H), 6.30 (ddd, *J* = 8.1, 2.3, 0.9 Hz, 2H), 3.83 (t, *J* = 7.2 Hz, 8H), 2.33 (p, *J* = 7.3 Hz, 4H); ^{13}C NMR ($CDCl_3$, 101 MHz) δ 152.8 (C), 136.3 (C), 129.5 (CH), 119.9 (CH), 113.6 (CH), 110.1 (CH), 52.5 (CH_2), 17.1 (CH_2); HRMS (ESI) calcd for $C_{18}H_{21}N_2S$ [M+H]$^+$ 297.1420, found 297.1428.

Bis(5-(azetidin-1-yl)-2-bromophenyl)sulfane (8)

Sulfide **17** (6.00 g, 20.2 mmol) was taken up in DMF (100 mL). *N*-Bromosuccinimide (7.20 g, 40.5 mmol, 2 eq) was added portion-wise over 5 min, and the reaction was then stirred at room temperature for 2 h. The reaction mixture was concentrated *in vacuo*; the resulting residue was diluted with water and extracted with EtOAc (2×). The combined organic extracts were washed with water and brine, dried over anhydrous MgSO$_4$, filtered, and concentrated *in vacuo*. The crude product was triturated with Et$_2$O, sonicated, and filtered. The filter cake was washed with Et$_2$O and dried to provide the title compound as a white solid. The filtrate was concentrated, chromatographed on silica gel (0–50% Et$_2$O/hexanes, linear gradient), and triturated as before to yield additional dibromide product. The two crops of white powder were combined, affording 6.51 g (71%) of dibromide **8**. ^{1}H NMR (CDCl$_3$, 400 MHz) δ 7.40 – 7.34 (m, 2H), 6.23 – 6.18 (m, 4H), 3.76 (t, *J* = 7.3 Hz, 8H), 2.31 (p, *J* = 7.2 Hz, 4H); ^{13}C NMR (CDCl$_3$, 101 MHz) δ 151.9 (C), 135.6 (C), 133.3 (CH), 115.0 (CH), 112.3 (C), 112.1 (CH), 52.4 (CH$_2$), 16.9 (CH$_2$); HRMS (ESI) calcd for C$_{18}$H$_{19}$Br$_2$N$_2$S [M+H]$^+$ 452.9630, found 452.9632.

JF$_{570}$ (10)

A solution of dibromide **8** (200 mg, 0.440 mmol) in THF (10 mL) was cooled to −78°C under nitrogen. *tert*-Butyllithium (1.7 M in pentane, 1.14 mL, 1.94 mmol, 4.4 eq) was added, and the reaction was stirred at −78°C for 30 min. It was then warmed to −20°C, and a solution of phthalic anhydride (**9**; 143 mg, 0.969 mmol, 2.2 eq) in THF (10 mL) was added dropwise over 30 min via addition funnel. The reaction was allowed to warm to room temperature overnight (18 h). Following the addition of AcOH (100 μL), the mixture was diluted with MeOH, deposited onto Celite, and concentrated to dryness. Silica gel chromatography (0–10% MeOH (2 M NH$_3$)/CH$_2$Cl$_2$, linear gradient; dry load with Celite) afforded 87 mg (46%) of JF$_{570}$ (**10**) as a dark purple solid. ^{1}H NMR (CD$_3$OD, 400 MHz) δ 8.14 – 8.08 (m, 1H), 7.68 – 7.59 (m, 2H), 7.25 (d, *J* = 9.3 Hz, 2H), 7.21 – 7.17 (m, 1H), 6.79 (d, *J* = 2.3 Hz, 2H), 6.55 (dd, *J* = 9.3, 2.3 Hz, 2H), 4.22 (t, *J* = 7.6 Hz, 8H), 2.51 (p, *J* = 7.6 Hz, 4H); ^{13}C NMR (CD$_3$OD, 101 MHz) δ 172.6 (C), 158.9 (C), 154.0 (C), 144.0 (C), 139.14 (C), 139.10 (C), 136.7 (CH), 131.3 (CH), 130.8 (C), 130.4 (CH), 130.3 (CH), 120.7 (C), 113.9 (CH), 104.6 (CH), 52.6 (CH$_2$), 16.9 (CH$_2$); Analytical HPLC: t$_R$ = 11.8 min, >99% purity (10–95% MeCN/H$_2$O, linear gradient, with constant 0.1% v/v TFA additive; 20 min run; 1 mL/min flow; ESI; positive ion mode; detection at 550 nm); HRMS (ESI) calcd for C$_{26}$H$_{23}$N$_2$O$_2$S [M+H]$^+$ 427.1475, found 427.1489.

6-Carboxy-JF$_{570}$ (19)

A solution of dibromide **8** (600 mg, 1.32 mmol, 1.5 eq) in THF (30 mL) was cooled to -78°C under nitrogen. *tert*-Butyllithium (1.7 M in pentane, 3.11 mL, 5.28 mmol, 6 eq) was added, and the reaction was stirred at -78°C for 30 min. It was then warmed to -20°C, and a solution of ester **18** (346 mg, 0.880 mmol, 1 eq) in THF (15 mL) was added dropwise over 30 min via addition funnel. The reaction was allowed to warm to room temperature overnight (18 h). It was subsequently diluted with saturated NH$_4$Cl and water and extracted with EtOAc (2×). The combined organic extracts were dried over anhydrous MgSO$_4$, filtered, and concentrated *in vacuo*. The resulting residue was redissolved in MeOH (10 mL), and 1 M HCl (1 mL) was added. After stirring the solution at room temperature for 30 min, it was diluted with toluene (10 mL), deposited onto Celite, concentrated to dryness, and purified by flash chromatography (0–20% MeOH/CH$_2$Cl$_2$, linear gradient, with constant 1% v/v AcOH additive; dry load with Celite) to provide the bis(2,2-bis(hydroxymethyl)propyl) diester intermediate (608 mg, 94%, acetate salt).

The diester (608 mg, 0.827 mmol) was taken up in 2,2,2-trifluoroethanol (15 mL), and 25% w/w NaOH (5 mL) was added. The reaction was stirred at room temperature for 7 days. It was then acidified with AcOH (5 mL), diluted with water, and extracted with 15% *i*-PrOH/CHCl$_3$ (3×). The combined organic extracts were dried over anhydrous MgSO$_4$, filtered, and evaporated. Flash chromatography on silica gel (0–20% MeOH/CH$_2$Cl$_2$, linear gradient, with constant 1% v/v AcOH additive) afforded 342 mg (78%, TFA salt) of 6-carboxy-JF$_{570}$ (**19**) as a dark purple solid. ^{1}H NMR (CD$_3$OD, 400 MHz) δ 8.41 (d, *J* = 8.2 Hz, 1H), 8.36 (dd, *J* = 8.2, 1.6 Hz, 1H), 7.87 (d, *J* = 1.6 Hz, 1H), 7.15 (d, *J* = 9.4 Hz, 2H), 6.88 (d, *J* = 2.3 Hz, 2H), 6.62 (dd, *J* = 9.4, 2.3 Hz, 2H), 4.27 (t, *J* = 7.7 Hz, 8H), 2.53 (p, *J* = 7.6 Hz, 4H); ^{13}C NMR (CD$_3$OD, 101 MHz) δ 167.8 (C), 167.3 (C), 161.8 (C), 154.3 (C), 144.9 (C), 139.1 (C), 136.5 (CH), 136.0 (C), 135.9 (C), 132.9 (CH), 132.5 (CH), 131.8 (CH), 120.1 (C), 114.8 (CH), 104.6 (CH), 52.7 (CH$_2$), 16.9 (CH$_2$); Analytical HPLC: t$_R$ = 9.8 min, >99% purity (10–95% MeCN/H$_2$O, linear gradient, with constant 0.1% v/v TFA additive; 20 min run; 1 mL/min flow; ESI; positive ion mode; detection at 575 nm); HRMS (ESI) calcd for C$_{27}$H$_{23}$N$_2$O$_4$S [M+H]$^+$ 471.1373, found 471.1376.

JF$_{570}$–HaloTag ligand (10$_{HTL}$)

6-Carboxy-JF$_{570}$ (**19**; acetate salt; 30 mg, 56.5 μmol) was combined with DSC (34.8 mg, 136 μmol, 2.4 eq) in DMF (2 mL). After adding Et$_3$N (47.3 μL, 339 μmol, 6 eq) and DMAP (0.7 mg, 5.7 μmol, 0.1 eq), the reaction was stirred at room temperature for 1 h. HaloTag(O2) amine (HTL-NH$_2$, **13**; TFA salt; 57.3 mg, 170 μmol, 3 eq) in DMF (250 μL) was added, and the reaction was stirred an additional 1 h at room temperature. Purification of the crude reaction mixture by reverse phase HPLC (10–95% MeCN/H$_2$O, linear gradient, with constant 0.1% v/v TFA additive) provided 32.2 mg (72%, TFA salt) of JF$_{570}$–HaloTag ligand (**10$_{HTL}$**) as a dark purple solid. ^{1}H NMR (CD$_3$OD, 400 MHz) δ 8.73 (t, *J* = 5.4 Hz, 1H), 8.40 (d, *J* = 8.2 Hz, 1H), 8.20 (dd, *J* = 8.3, 1.8 Hz, 1H), 7.75 (d, *J* = 1.7 Hz, 1H), 7.16 (d, *J* = 9.4 Hz, 2H), 6.90 (d, *J* = 2.3 Hz, 2H), 6.62 (dd, *J* = 9.4, 2.3 Hz, 2H), 4.28 (t, *J* = 7.6 Hz, 8H), 3.68 – 3.55 (m, 8H), 3.53 (t, *J* = 6.6 Hz, 2H), 3.42 (t, *J* = 6.5 Hz, 2H), 2.54 (p, *J* = 7.6 Hz, 4H), 1.76 – 1.67 (m, 2H), 1.54 – 1.45 (m, 2H), 1.45 – 1.29 (m, 4H); Analytical HPLC: t$_R$ = 12.5 min, >99% purity (10–95% MeCN/H$_2$O, linear gradient, with constant 0.1% v/v TFA additive; 20 min run; 1 mL/min flow; ESI; positive ion mode; detection at 575 nm); HRMS (ESI) calcd for C$_{37}$H$_{43}$ClN$_3$O$_5$S [M+H]$^+$ 676.2606, found 676.2622.

Spectroscopy

Spectroscopy of various dyes, photosensitizers and associated HaloTag Ligand variants was performed using 1 cm path length, 3.5 mL or 1 mL or 300 μL quartz cuvettes (Starna Cells). Absorption spectra were recorded on a Cary Model 100 spectrometer (Agi-

lent). Fluorescence emission spectra were recorded on a Varian Cary Eclipse (Agilent). Absorbance and fluorescence spectroscopy were also carried out using a Flexstation 3 microplate reader (Molecular Devices) when noted. Fluorescence quantum yields were recorded on a Quantaurus-QY (Hamamatsu). Spectroscopy measurements of free dyes were performed 10 mM HEPES, pH 7.3 at ambient temperature ($22 \pm 2°C$); the reported values of maximum absorption wavelength (λ_{abs}), extinction coefficient at λ_{abs} (ϵ), maximum fluorescence emission wavelength (λ_{em}), and fluorescence quantum yield (Φ_f) are averages ($n = 3$). Spectroscopy of HaloTag conjugates were performed in Dulbecco's phosphate-buffered saline (DPBS, Gibco).

Solutions prepared for spectroscopy contained 3–5 μM dye and 10 μM HaloTag protein when applicable. Spectra of compounds bound to HaloTag protein were allowed a 30 min binding incubation period in the dark at ambient temperature prior to measurement. Masked compound Eosin-Ac$_2$–HaloTag ligand (**2$_{HTL}$Ac$_2$**) was incubated with 23.75 units/mL porcine liver esterase in the dark at ambient temperature for 6 h prior to incubation with HaloTag protein and subsequent spectroscopy. The reported values of maximum absorption wavelength (λ_{abs}), extinction coefficient at λ_{abs} (ϵ), maximum fluorescence emission wavelength (λ_{em}), and fluorescence quantum yield (Φ_f) are averages ($n = 2$)

K_{L-Z} was calculated using the following formula: $K_{L-Z} = (\epsilon_{dw}/\epsilon_{max})/(1 - \epsilon_{dw}/\epsilon_{max})$, where ϵ_{dw} is the extinction coefficient in a 1:1 v/v dioxane:water solvent mixture, and ϵ_{max} is the extinction coefficient in 0.1% v/v trifluoroacetic acid (TFA) in 2,2,2-trifluoroethanol (TFE). The reported values are averages ($n = 2$).

HaloTag Protein Purification

Purified HaloTag protein was obtained via pRSET vector expression in BL21 *E. coli* and subsequent purification via immobilized metal affinity chromatography (IMAC) using an ÄKTA Avant (GE Healthcare Life Sciences). Protein was dialyzed in DPBS for 48 h prior to quantification and use.

Singlet Oxygen Quantum Yield

Singlet oxygen quantum yields (Φ_{SO}) of free dyes were measured using the commercially available Singlet Oxygen Sensor Green (SOSG; Thermo Fisher). Solutions of 5 μM dye + 30 μM SOSG in DPBS + 0.1% DMSO dye cosolvent + 0.6% MeOH SOSG cosolvent at a volume of 30 μL were excited in 384-well microplate wells with light doses of increasing exposure times and constant power on a Nikon Ti-Eclipse microscope outfitted with a Lumencor LED excitation system. SOSG emission was measured using a FlexStation 3 microplate reader and corrected for baseline emission and DMSO negative control contributions to emission. Values were first normalized to the estimated photons absorbed by each dye to correct for differential excitation efficiency based upon light source output spectra and dye molar absorptivity spectra; absorption cross-section measurements of dyes for Φ_{SO} determination were measured in DPBS. Well averages were then calculated ($n = 3$), and data were normalized to the standard dye Rose Bengal (**3**), which has a $\Phi_{SO} = 0.76$ (Ezquerra Riega et al., 2017).

Chromophore Assisted Light Inactivation (CALI) of EGFP in Live Cells

U2OS cells were transfected with pHaloTag-EGFP (Ebner et al., 2017) via the Amaxa Nucleofector II system from Lonza to transiently express a HaloTag-EGFP fusion protein. These cells were labeled with 1 μM ligand in media + 0.1% DMSO cosolvent for 1 h followed by 2 media washes. EGFP fluorescence was imaged via 488 nm laser or 440 nm-centered excitation preceding and immediately following a 10 s exposure to 10 W/cm^2 561 nm monochromatic (laser) or 508 nm-centered LED-based light; the 440 nm/508 nm combination was utilized for the Eosin-Ac$_2$–HaloTag ligand (**2$_{HTL}$Ac$_2$**). Change in mean EGFP signal due to CALI was calculated per manually segmented cell using the FIJI 2.0.0-rc-69/1.52i distribution of ImageJ (Schindelin et al., 2012).

Photoablation of Cells in Culture

U2OS cells expressing HaloTag–H2B (Chen et al., 2014), HaloTag–TOMM20, or no exogenous proteins were seeded in a 384-well, tissue-culture treated microplate (Perkin Elmer) at a density of 2K cells/well and allowed to grow for 24 h. Cells were then labeled with 1 μM ligand in media + 0.1% DMSO cosolvent for 1 h followed by 2 media washes and exposed to various light of various power and wavelength for 3 min, one well at a time, through the 4× objective of a Nikon Ti-Eclipse microscope at 5% CO$_2$, 37°C. After an additional incubation for 24 hr, cells were costained with NucBlue Live ReadyProbes Reagent and NucRed Dead 647 ReadyProbes Reagent (Thermo Fisher) and imaged. The images were analyzed using the FIJI 2.0.0-rc-69/1.52i distribution of ImageJ (Schindelin et al., 2012) as follows. Image segmentation was carried out by autothresholding each image via the Triangle algorithm ± 10 manual value adjustments until image noise was optimally suppressed followed by the binary watershed algorithm. Segmented cells were counted via the Analyze Particles function (5-inf pixel size, 0.15–1.00 roundness). The percentage of ablated cells was determined by measuring the number of dead cells stained in the NucRed Dead 647 ReadyProbe image and the total number of cells stained in the NucBlue Live ReadyProbe image. For the representative confocal and brightfield images (Figures 2H and 2I) U2OS cells expressing HaloTag–TOMM20 were labeled with 500 nM ligand in media, washed, and imaged using a Zeiss 880 inverted confocal microscope with an EC Plan-Neofluar 40×/1.30 oil immersion objective and 561 nm laser excitation. Cells were imaged before and 30 min after a 3 min irradiation dose delivered with an X-Cite 120PC Series illuminator using Zeiss filter set 45 (excitation: 560 nm with a 40 nm bandpass; beamsplitter: 585 nm; emission: 630 nm with a 75 nm bandpass).

Cloning of Zebrafish Ablation Construct

The zebrafish construct 10×UAS:TOMM20-HaloTag-p2a-mCerulean3, myl7:EGFP was assembled using the Tol2kit system with Gateway LR Clonase II Enzyme Mix (Invitrogen). It was composed of the following components: p5E 10×UAS, pME TOMM20-HaloTagv7-p2a-mCerulean3, p3E PolyA (Tol2#302) and the destination vector, pDestTol2pCG2 (Tol2#395) (Grzegorski et al., 2014; Kwan et al., 2007; Lo et al., 2015; Los et al., 2008; Markwardt et al., 2011).

In Vivo Ablation of Zebrafish Neurons

$Mitfa^{w2/w2}$ $roy^{a9/a9}$ (Casper) zebrafish (Kimura et al., 2008) were maintained under standard conditions at 28.5°C and a 14:10 h light:dark cycle. Embryos (1–2 cell stage) of Tg(elavl3:Gal4-VP16) (Kimura et al., 2008) were injected with 25 ng/μL DNA plasmid encoding the co-expression cassette of mitochondria-localized HaloTag and mCerulean3 under the control of the 10×UAS promoter (10×UAS:TOMM20-HaloTag-p2a-mCerulean3, myl7:EGFP), and 25 ng/μL Tol2 transposase mRNA diluted in E3 medium. Subsequently, the injected embryos with broad expression of mCerulean3 were incubated in system water containing HaloTag dye ligands: JF$_{570}$–HaloTag ligand (**10$_{HTL}$**) or JF$_{585}$–HaloTag ligand (**20$_{HTL}$**) at 30 μM at 4-day post-fertilization (dpf) for 12 h and then washed in dye-free system water. Larvae at 5 dpf were then anesthetized in tricaine methanesulfonate (MilliporeSigma, E10521, MO) dissolved in system water at 160 mg/L and then embedded in 1.6% low melting point agar (MilliporeSigma, 2070-OP, MO). Volumetric images of the entire brain were first acquired with a confocal microscope (Zeiss, LSM880) with a 20× 1.0 NA objective lens (Zeiss, W Plan-Apochromat 20×/1.0) to confirm the distribution of the cells labeled with mCerulean3 and HaloTag ligand prior to ablation. Then yellow, 560 nm-centered ablation light was shone on the forebrain region (Figures 3A and 3B; Zone 1) for 5 minutes through the widefield illumination path equipped with a fluorescent filter (Zeiss, Filter Set 45) and a mercury lamp (Leistungselektronik JENA GmbH, HXP 120 V) with the field diaphragm adjusted just to illuminate the target region. The power densities used for **10$_{HTL}$** and **20$_{HTL}$** 3 W/cm^2 and 12 W/cm^2 respectively. Post-ablation confocal stacks were acquired right after the ablation and 1 day after the ablation (6 dpf) with the imaging parameters identical to those used prior to ablation. Images were analyzed using the FIJI 2.0.0-rc-69/1.52i distribution of ImageJ (Schindelin et al., 2012) as follows. Zone ROIs were manually segmented using brightfield maximum intensity z-projections and kept consistent across image stack channels using FIJI's ROI manager and crop function. FIJI's 3D Object Counter module was utilized to count cells in the mCer fluorescence channel image stacks obtained pre-irradiation and 24 h post-irradiation using an 8-bit minimum threshold pixel value of 11 and default size settings. The percentage of remaining cells was determined by measuring the number of cells in pre-irradiation samples and the number of cells in 24 h post-irradiation samples.

DAB Photopolymerization for Electron Microscopy

HOS cells were incubated for 30 min with 5 μM dye in culture medium at 37°C. Cells were fixed with 4% paraformaldehyde (Electron Microscopy Sciences) in 5 mM CaCl$_2$, 0.1 M sodium cacodylate buffer, pH 7.4, incubating at room temperature for 5 min and 0°C (ice) for 2 h. Cells were washed 5×, 2 min each wash, in 0.1 M sodium cacodylate buffer and then blocked for 15 min in blocking buffer (10 mM glycine, 10 mM potassium cyanide in 0.1 M sodium cacodylate buffer). After 3× washes with 0.1 M sodium cacodylate buffer, cells were bathed in 2.5 mM DAB·(HCl)$_4$ (Sigma) in 0.1 M sodium cacodylate buffer. Cells were placed on a cold-stage Leica SPE-II confocal microscope and photooxidized by continuous epi-fluorescence illumination (150 W Xenon Lamp) through an mCherry filter cube (excitation: 542–582 nm) for 7 min. Cells were washed 5×, 2 min each wash, with 0.1 M sodium cacodylate buffer and fixed for 30 min with 2% glutaraldehyde at 4°C. After 3× additional washes with 0.1 M sodium cacodylate buffer, the sample was stained for 30 min with 1% osmium tetroxide and 1.5% potassium ferrocyanide in 0.1 M sodium cacodylate buffer. Cells were washed with doubly distilled water 5×, 2 min each wash.

EM Sample Preparation and Imaging

After DAB polymerization and osmification, HOS cells were dehydrated in ethanol and embedded in Durcupan epoxy resin as described previously (Ou et al., 2015). Briefly, the samples were incubated for 2 min in water containing increasing concentrations of ethanol (20% v/v, 50% v/v, 70% v/v, and 90% v/v) followed by three successive 2 min incubations in 100% ethanol. The samples were then infiltrated with durcupan resin (Sigma, 44610) with three successive 2 h treatments. Finally, the cells were incubated with freshly prepared durcupan resin and cured for 2 d at 60°C. Epoxy embedded cells were cut into either 70–80 nm sections and mounted onto 200 hexagonal mesh copper grid for TEM or 250 nm sections mounted onto slot grid covered with a luxel film for electron tomography. For conventional transmission electron microscopy (TEM), ultrathin sections were imaged at 80 kV using an FEI Tecnai microscope (FEI Company). For EM tomography, a mixture of 5 nm and 10 nm colloidal gold particles serving as fiducial markers were deposited on both sides of the semi-thin (∼250 nm) specimen sections after the sample grids were glow discharged. The tomography data was collected on an FEI Titan Halo electron microscope operating at 300 kV with a DE64 direct electron detector. The grids were loaded into a rotation holder specifically designed for multi-tilt tomography manufactured by Fischione Instruments (Model 2040). During a tilt series, images were acquired tilting the goniometer holding the sample holder from −60° to +60° with 0.5° increments. SerialEM was used to control the FEI Titan for the data acquisition (Mastronarde, 1997). The sample was rotated along the z-axis by 45° for the second tilt series, 90° (relative to origin) for the third tilt series, and 135° (relative to origin) for the final tilt series. Adjustments were made to the stage/sample height to ensure an identical eucentric height and magnification for each tilt series. The sequence of tilt series followed the multilevel access scheme previously described (Phan et al., 2017), which minimizes errors associated with sample shrinkage evenly across all tilt series. EM tomography reconstruction: The entire set of EMT images were

aligned and reconstructed using Transform-based Tracking, Bundle adjustment, and Reconstruction (TxBR) package (Lawrence et al., 2006; Phan et al., 2012, 2017). 3D volume rendering was made with Amira 6.3.

QUANTIFICATION AND STATISTICAL ANALYSES

For spectroscopy measurements, *n* values are given in the Method Details section and represent the number of measurements of different samples prepared from the same dye DMSO stock solution or HaloTag conjugate stock solution. For Φ_{SO} determination, *n* values are given in the Method Details section and represent the number of separate photochemical experiments using the same dye DMSO stock solutions of dye and SOSG sensor. For CALI experiments, *n* values are given in the legend of Figure 2 and represent the number of cells. For ablation experiments in culture, *n* values are given in the legends of Figure 2 and Figure S3 and represent the number of separate experiments counting all and dead cells using NucBlue Live and NucRed Dead. For ablation experiments *in vivo*, *n* values are given in the legend of Figure 3 and indicate the number of fish. For electron microscopy experiments, these were duplicated with similar results as indicated in the legend of Figure 4. For all whisker plots, the center line indicates median; box limits indicate upper and lower quartiles; whiskers indicate min–max. Graphs were rendered using GraphPad Prism 7.04. Statistical tests were performed using the Addinsoft XLSTAT v2020.1.1 add-in to Microsoft Excel 2019 v1908 build 11929.20838. All data analyzed statistically were assessed for normality and scedasticity assumptions when appropriate using the Shapiro-Wilk test or Levene's test. Parametric or non-parametric tests are indicated in the figure legends and include the Student's T-test, Mann–Whitney U test, ANOVA with Tukey's post-hoc, Welch's ANOVA with Games–Howell post-hoc, and Kruskal–Wallis H test with Steel–Dwass–Critchlow–Fligner procedure.